


## RESEARCH ARTICLE

# Biphasic regulation of RNA interference during rotavirus infection by modulation of Argonaute2

Urbi Mukhopadhyay<sup>1</sup> | Shampa Chanda<sup>2</sup> | Upayan Patra<sup>1</sup> | Anupam Mukherjee<sup>1</sup> | Satoshi Komoto<sup>3</sup> | Mamta Chawla-Sarkar<sup>1</sup> 

<sup>1</sup>Division of Virology, National Institute of Cholera and Enteric Diseases, Kolkata, India

<sup>2</sup>Department of Biotechnology, GITAM Institute of Science, Visakhapatnam, India

<sup>3</sup>Department of Virology and Parasitology, School of Medicine, Fujita Health University, Aichi, Japan

## Correspondence

Mamta Chawla-Sarkar, Division of Virology, National Institute of Cholera and Enteric Diseases, P-33, C.I.T. Road, Scheme-XM, Beliaghata, Kolkata 700010, West Bengal, India  
Email: chawlam70@gmail.com; chawlasarkar.m@icmr.gov.in

## Funding information

Okayama University Project through Japan Initiative for Global Research Network on Infectious Diseases (J-GRID) of the Agency for Medical Research and Development (AMED); Science and Engineering Research Board; Dept. of Science and Technology (DST-SERB), Grant/Award Number: EMR/2016/001361

## Abstract

RNA interference (RNAi) is an evolutionary ancient innate immune response in plants, nematodes, and arthropods providing natural protection against viral infection. Viruses have also gained counter-defensive measures by producing virulence determinants called viral-suppressors-of-RNAi (VSRs). Interestingly, in spite of dominance of interferon-based immunity over RNAi in somatic cells of higher vertebrates, recent reports are accumulating in favour of retention of the antiviral nature of RNAi in mammalian cells. The present study focuses on the modulation of intracellular RNAi during infection with rotavirus (RV), an enteric virus with double-stranded RNA genome. Intriguingly, a time point-dependent bimodal regulation of RNAi was observed in RV-infected cells, where short interfering RNA (siRNA)-based RNAi was rendered non-functional during early hours of infection only to be reinstated fully beyond that early infection stage. Subsequent investigations revealed RV non-structural protein 1 to serve as a putative VSR by associating with and triggering degradation of Argonaute2 (AGO2), the prime effector of siRNA-mediated RNAi, via ubiquitin-proteasome pathway. The proviral significance of AGO2 degradation was further confirmed when ectopic overexpression of AGO2 significantly reduced RV infection. Cumulatively, the current study presents a unique modulation of host RNAi during RV infection, highlighting the importance of antiviral RNAi in mammalian cells.

## KEYWORDS

Argonaute2, nonstructural protein 1, RNA interference, rotavirus, viral-suppressors-of-RNAi

## 1 | INTRODUCTION

RNA interference (RNAi) is an evolutionary-conserved homology-dependent gene-silencing mechanism, which governs posttranscriptional regulation of a myriad of cellular genes, heterochromatization, and antiviral innate immunity (Bartel, 2018; Baulcombe, 2004; Hannon, 2002). It is the lattermost function, however, for which RNAi is postulated to have primarily evolved an intrinsic RNA surveillance system serving as a natural immune safeguard against invading nucleic

acids of transposons and viral origin (van Rij & Andino, 2006). The working principle of RNAi essentially includes cleavage (dicing) of double stranded RNAs (dsRNAs) of endogenous (during microRNA biogenesis) or exogenous (foreign nucleic acids) origin by cellular RNase III-like endonuclease DICER into small RNA duplexes of approximately 21–23 nucleotides (mature microRNAs and short interfering RNAs). These RNA duplexes with characteristic terminal overhangs are further loaded on to a supramolecular RNA-induced silencing complex (RISC), where one strand of the duplex is stripped off (passenger strand), and the other strand (guide RNA) bearing complementarity to cognate mRNA sequence guides the silencer complex

Urbi Mukhopadhyay and Shampa Chanda have equal contributions to this work.

to its target. The ultimate fate of the target mRNA is determined by the degree of complementarity between the guide strand and the target sequence; perfect complementarity (for siRNAs) triggers cleavage (slicing) of the mRNA whereas imperfect complementarity (generally for miRNAs) sequesters mRNA away from polyribosomes into cytoplasmic processing bodies (P bodies) resulting in translational repression. At the catalytic core of RISC are the Argonaute (AGO) family of proteins of which mammals encode four homologs (AGO1–4). In spite of evidences of functional redundancy among the four AGOs, slicer activity is exhibited only by the isoform AGO2 in mammalian cells (Bartel, 2009; Bartel, 2018; Siomi & Siomi, 2009).

During viral infection, replicative or transcriptive viral dsRNA intermediates may succumb to processing by host cellular RNAi yielding virus-derived small interfering RNAs (viRNAs), which might further direct viral RNA cleavage ultimately resulting in heavily attenuated viral replication. As a coevolutionary counterstrategy, viruses have adopted RNAi-evasive virulence measures in the form of producing virus-encoded-suppressors-of-RNAi (Bivalkar-Mehla et al., 2011; Burgyán & Havelda, 2011; Ding, Han, Wang, & Li, 2018; Wu, Wang, & Ding, 2010). Experimental evidence of viRNA generation during the course of natural viral infection is abundant in plants, worms, and insects (Siu et al., 2011). Physiological relevance of RNAi as an antiviral innate immunity, however, has been greatly debated in differentiated, somatic cells of higher vertebrates because of the evolution of a superior, interferon (IFN)-based innate immune system (Cullen & Cherry, 2013; Goubau, Deddouche, & e Sousa, 2013; Maillard et al., 2016; Samuel, 2001; Schneider, Chevillotte, & Rice, 2014; ten Oever, 2016). Alternatively, mammalian viruses, at least in some contexts, have been experimentally shown to exert strong RNAi evasive mechanisms by encoding highly potent VSRs (Li, Lu, Han, Fan, & Ding, 2013; Qiu et al., 2017), justifying near absence of viRNAs in mammalian cells during natural course of infection (Parameswaran et al., 2010). Mammalian VSRs characterised till date include ebola virus VP35 (Haasnoot et al., 2007), influenza A virus NS1 (Bucher, Hemmes, de Haan, Goldbach, & Prins, 2004), vaccinia virus E3L (Li et al., 2004), nodamura virus B2 (Johnson, Price, Eckerle, & Ball, 2004), hepatitis C virus core (Wang et al., 2006), HIV-1 Tat (Bennasser & Jeang, 2006; Bennasser, Le, Benkirane, & Jeang, 2005), coronavirus nucleocapsid protein N (Cui et al., 2015), and virus-associated RNAi and RNAII of adenoviruses (Andersson et al., 2005; Lu & Cullen, 2004). VSRs are generally dsRNA-binding proteins (excepting adenoviral VSR), which inhibit activity of either Dicer, AGO, or both. Interestingly, all VSRs identified from mammalian viruses possess IFN or protein kinase R antagonistic properties and are essential for replication and pathogenesis, suggesting that RNAi and other innate antiviral responses are interrelated.

The genome of rotavirus (RV), a diarrheagenic virus in infants and young animals, consists of 11 segmented double-stranded RNAs, which are usually enclosed within viral double-layered particles and, at proliferative stage of infection, within highly dynamic encagements called viroplasm. Single-stranded viral mRNAs, produced within double-layered particles, are either translated into six structural (VP1

to VP4, VP6, and VP7) and six nonstructural (NSP1 to NSP6) proteins or used as templates for viral RNA replication (Desselberger, 2014; Estes & Greenberg, 2013). However, oozing of rotaviral dsRNA intermediates in unmasked cytosolic environment has been hypothesised based on RNase III-sensitive and dsRNA-positive scattered signals in infected host cell cytoplasm (Rojas, Arias, & López, 2010; Zhu et al., 2017). Accidental exposure of viral genomic dsRNAs or even transcriptive dsRNA intermediates in the cytoplasm may potentially evoke RNAi-based surveillance mechanism. Strikingly, previous reports emphasised retention of competent RNAi pathway in the context of RV infection enabling functionality of both small interfering RNAs (siRNAs) and short hairpin RNAs (shRNAs; Déctor, Romero, López, & Arias, 2002; Arias et al., 2004; López, Rojas, Ayala-Bretón, López, & Arias, 2005; Chen et al., 2011). Indeed, successfully knocking down expression of viral and host proteins has been proven to be excellent loss-of-function studies to unravel complex host–RV interaction networks (Dhillon & DurgaRao, 2018; Mukherjee, Patra, Bhowmick, & Chawla-Sarkar, 2018; Ocegüera, Peralta, Martínez-Delgado, Arias, & López, 2018; Patra, Mukhopadhyay, Sarkar, Mukherjee, & Chawla-Sarkar, 2019; Silva-Ayala et al., 2013; Trujillo-Alonso, Maruri-Avidal, Arias, & Lopez, 2011; Yin et al., 2018). Moreover, RNAi-based potential therapeutic approaches targeting RV genes have also been advocated (Arias et al., 2004). Notably, in most of these experiments, RNAi functionality was assessed at relatively late hours of infection (beyond 6-hr postinfection).

While studying loss-of-function attributes of selected cellular determinants in context of RV-SA11 infection, intriguingly, we found differential sensitivity of cellular genes to RNAi at different time points of infection. RNAi pathway was found to be inhibited during early hours (2–6 hr) of RV-SA11 infection only to be restored to full functional competence beyond that early phase. Blocking of RNAi was confirmed in the form of ablated functioning of siRNA and shRNA but not miRNA. Interestingly, hindrance to RNAi during the early stage of RV-SA11 infection coincided with the loss of protein level of AGO2. Further mechanistic studies revealed that RV-NSP1 interacts with and degrades AGO2 in ubiquitin–proteasome-dependent way. Together, the data highlight a fascinating and unique modulation of RNAi pathway in response to RV infection.

## 2 | RESULTS

### 2.1 | Host RNAi is blocked during early hours of RV infection

To assess the sensitivity of ectopic GFP expression to synthetic siRNA during early and late hours of RV infection, GFP (pEGFP-N1)-transfected MA104 cells were cotransfected with either siGFP or scrambled siRNA, and 36-hr posttransfection cells were further mock-infected or infected with RV-SA11 for 3 and 9 hr. Interestingly, analyses of GFP expression by immunoblotting showed siRNA-mediated targeted knock-down of GFP to be apparent in mock-infected cells as well as in cells infected with RV-SA11 for

9 hr but not in RV-SA11-infected cells harvested at 3-hr postinfection (3 hpi; Figure 1a). We ruled out transfection of siGFP to have any off-target effects on overall RV infection as relative expression of RV structural and nonstructural proteins remained unperturbed (Figure 1a; Figure S1A). Visualisation by immunofluorescence microscopy (10 $\times$  magnification) in MA104 cells (Figure 1b) and HEK293 cells (Figure S1B) also revealed ectopic expression of GFP to be sensitive to RNAi only at 9 hpi but not at 3 hpi, suggesting time point-dependent differential regulation of RNAi during RV-SA11 infection. Rhodamine-conjugated NSP5 visualised in RV-infected

samples under higher magnification (63 $\times$  oil immersion) ensured progressive infection (Figure 1b, panel 5). Next, we investigated whether RNAi targeted against any endogenous cellular protein was also regulated similarly during early and late hours of RV-SA11 infection. MA104 cells, transfected with scrambled siRNA or RING-box protein 1 (Rbx1)-specific siRNA for 36 hr, were subsequently mock-infected or infected with RV-SA11. Consistent to our previous results, Rbx1 expression was successfully knocked down in response to Rbx1 siRNA in RV-SA11-infected cells lysed at 9 hpi as well as in mock-infected control but not in RV-SA11-infected cells harvested

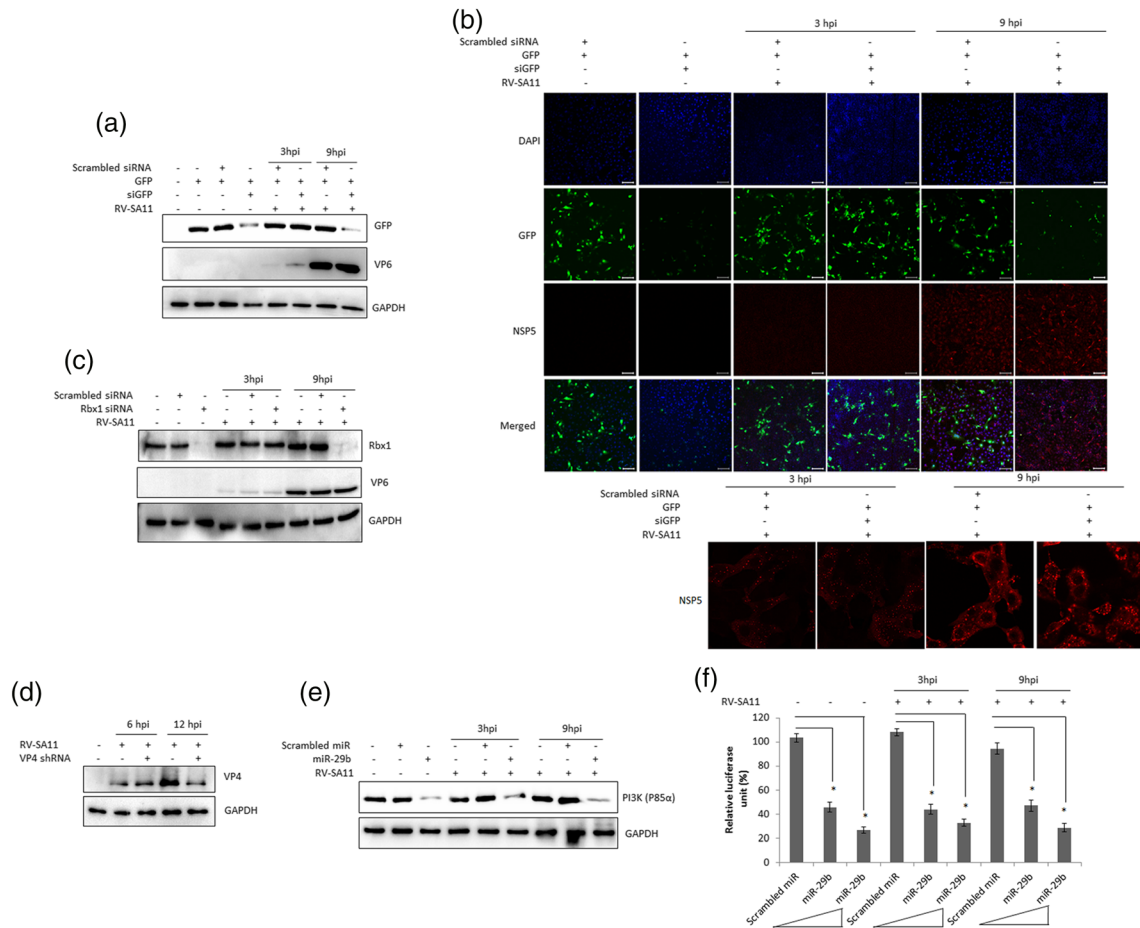


**FIGURE 1** Host RNA interference is blocked during early hours of RV-SA11 infection. (a) MA104 cells transfected with GFP (pEGFP-N1) were further cotransfected with scrambled siRNA or siGFP as indicated in the figure (designated by +, -); 36-hr posttransfection, cells were mock infected or infected with RV-SA11. After 3 and 9 hpi, cells were harvested, and GFP expression was analysed by western blot analysis. (b) GFP (pEGFP-N1)-transfected MA104 cells were cotreated with scrambled siRNA or siGFP as indicated in the figure (designated by +, -). Cells were fixed at indicated time points postinfection (mock/RV-SA11) with paraformaldehyde, permeabilised, blocked, and subsequently stained overnight with anti-NSP5 antibody (as a marker of virus infection). Secondary staining and mounting were performed with Rhodamine conjugated anti-rabbit antibody and DAPI, respectively. Cells were finally visualised by confocal microscopy (10 $\times$ ); Scale bar 100  $\mu$ m. (Lower panel) Rhodamine-conjugated NSP5 was visualised in RV-infected samples under higher magnification to ensure progressive infection (63 $\times$  oil immersion). (c) MA104 cells were transfected with scrambled siRNA or Rbx1 siRNA. 36-hr posttransfection, cells were either mock infected or infected with RV-SA11 for indicated time points; Rbx1 expression was finally assessed by immunoblot analysis. (d) MA104 cells, transfected with either empty vector (PLKO.1-TRC) or RV-VP4-shRNA (cloned into PLKO.1-TRC vector) for 24 hr, were further infected with RV-SA11 for 6 and 12 hr. Expression of RV-VP4 in whole cellular extracts was checked by western blot analysis. (e) Scrambled miR/miR-29b mimic transfected MA104 cells were mock infected or infected with RV-SA11 for 3 and 9 hr. Cellular lysates prepared at indicated time points were subjected to western blot analysis to check expression of P85 $\alpha$  subunit of PI3K. (f) pMIR-REPORT Luciferase construct containing the 3'-UTR of P85 $\alpha$ -PI3K was transfected in HEK293 cells in association with miR-29b mimic (20 and 40 nM). 36-hr posttransfection, cells were either kept mock-infected or infected with RV-SA11 for 3 and 9 hr. Percentage of relative luciferase activity was finally represented after normalising Firefly luciferase with corresponding Renilla luciferase control

at 3 hpi (Figure 1c), further indicating hindrance of RNAi mechanism during early hours of RV-SA11 infection. Furthermore, sensitivity of RV protein expression to shRNA-mediated RNAi in infection scenario was analysed. MA104 cells expressing shRNA against VP4 for 24 hr were subsequently infected with RV-SA11, and expression of VP4 was checked after 6 and 12 hr of infection. In agreement with previous reports (Arias et al., 2004; Déctor et al., 2002), expressions of VP4 RNA and protein were found to be silenced at 12 hpi (Figure S1C; Figure 1d), suggesting sensitivity of viral protein expression to RNAi at late phase of RV-SA11 infection. Interestingly, shRNA-mediated silencing of VP4 expression was attenuated at 6 hpi (Figure S1C; Figure 1d), affirming our previous observation that functional competence of siRNA is lost during early phase of RV-SA11 infection.

We further checked modulation of miRNA-mediated RNAi by evaluating target repression capacity of ectopically administered miRNA mimic during early and late hours of RV-SA11 infection. MA104 cells, transfected with either miR-29b mimic or scrambled miR for 36 hr, were subsequently infected with RV-SA11 for 3 and 9 hr. One set of transfected cells was mock infected. Interestingly, following miR-29b overexpression, reduction of miR-29b target P85 $\alpha$  subunit of PI3K (Park, Lee, Ha, Nam, & Kim, 2009) was evident in both mock-infected cells and RV-infected cells for 3 (early time point) and 9 hr (late time point; Figure 1e). Consistently, much alike to mock-infected group, sensitivity of luciferase expression from pMIR-REPORT Luciferase vector containing 3'-UTR of P85 $\alpha$  subunit of PI3K in HEK293 cells to cotransfected miR-29b mimic (20 and 40 nM) was also found to be unaffected at both early (3 hpi) and late (9 hpi) hours of RV-SA11 infection (Figure 1f). Collectively, the results suggest that though inhibition of siRNA and shRNA-mediated RNAi occurs during early hours of RV-SA11 infection, functionality of miRNA is retained during the same infection window.

## 2.2 | Protein levels of AGO2 decline during early hours of RV infection

Differential regulation of RNAi pathway during early and late hours of RV-SA11 infection prompted us to investigate overall modulation of AGO family of proteins and Dicer in response to RV-SA11 infection in a time point-dependent manner. Interestingly, compared with the corresponding mock-infected controls, cellular protein levels of AGO2 decreased during 2–6-hr post RV-SA11 infection in MA104 (Figure 2a), HT29 (Figure S2A), and HEK293 (data not shown) cell line. At relatively late time points of infection ( $\geq 8$  hpi), protein level of AGO2 was restored (Figure 2a; Figure S2A). However, AGO1 protein level was found to be reduced during late hours of RV-SA11 infection (9–12 hpi; Figure 2a; Figure S2A). Levels of AGO3 and AGO4, two other members of AGO family proteins in mammals, as well as DICER, remained unchanged with respect to their respective mock-infected controls throughout indicated time period (2–12 hpi) of RV-SA11 infection (Figure 2a; Figure S2A). Confocal microscopy and subsequent quantitation of corrected total cell fluorescence (CTCF) also

revealed AGO2 expression to get reduced at 3 hpi compared with the mock-infected control only to restore and be distinctly visible again at 9 hpi (Figure 2b). Intracellular distribution of AGO2, however, was found to be somewhat different at 9 hpi from that in mock-infected control (Figure 2b). Furthermore, infection with UV-treated RV-SA11 (Smirnov, Kapituets, Amitina, Ginevskaya, & Kaverin, 1991) had no effect on AGO2 protein levels postinfection (Figure S2B). Together, the data suggest that actively replicating RV-SA11 triggers attenuation in protein levels of AGO2 leading to functional blocking of RNAi during early time points (2–6 hpi) of infection.

## 2.3 | RV nonstructural protein 1 triggers degradation of AGO2 by ubiquitin–proteasome system

We further speculated involvement of viral protein(s) in mediating reduction of AGO2 protein levels during 2–6-hr post RV-SA11 infection. Owing to previous reports of RV-NSP1 being involved in triggering degradation of multitude of host proteins, which are regulators of host cellular innate immunity (Arnold, Barro, & Patton, 2013; Bagchi, Bhowmick, Nandi, Kant Nayak, & Chawla-Sarkar, 2013; Barro & Patton, 2007; Bhowmick, Halder, Chattopadhyay, Nayak, & Chawla-Sarkar, 2013; Bhowmick, Mukherjee, Patra, & Chawla-Sarkar, 2015; Graff, Ettayebi, & Hardy, 2009; Graff, Ewen, Ettayebi, & Hardy, 2007; Graff, Mitzel, Weisend, Flenniken, & Hardy, 2002; Qin et al., 2011), the involvement of RV-NSP1 was investigated in the process. RV-NSP1, but not RV-NSP4, overexpression by itself resulted in significant reduction of AGO2 protein level in MA104 (Figure 3a) cell line. Decrease of Pan3 (Bhowmick et al., 2015) and induction of Ser616 phosphoDrp1 (Ser616 pDrp1; Mukherjee et al., 2018) served as positive controls for RV-NSP1 and RV-NSP4 overexpression, respectively (Figure 3a). RV-NSP1-mediated degradation of AGO2 was also evident in HEK293 cells transfected with pcDNSP1 (Figure S3A). AGO1 levels, however, remained unchanged in RV-NSP1-overexpressing cells (Figure 3a). Of note, overexpression of none of the other RV structural and nonstructural proteins resulted in AGO2 protein level reduction when transfected individually (data not shown). Gradual reduction of AGO2 protein levels in a dose-dependent manner in response to escalated concentration of transfected RV-NSP1 further ascertained the role of this viral NSP in modulating AGO2 levels (Figure S3B). Furthermore, infection with bovine RV strain A5–13 possessing wild-type NSP1 (Taniguchi, Kojima, & Urasawa, 1996) also resulted in reduced AGO2 protein levels (2–6 hpi) whereas corresponding NSP1 mutant RV strain A5–16 (Taniguchi et al., 1996) failed to decrease AGO2 during the same infection window (Figure 3b). Time kinetics of NSP1 mRNA and protein expression in RV-A5–13- and RV-SA11-infected cells showed gradual accumulation as a function of time point postinfection (Figure S3C; Figure 3b).

Subsequent investigations revealed that irreversible inhibition of proteasome with 1  $\mu$ M of lactacystin prevented RV-NSP1-mediated decline of AGO2 levels (Figure 3c). This was also supported by similar restoration of AGO2 protein levels in RV-NSP1-transfected cells in response to 5  $\mu$ M of reversible proteasome inhibitor MG-132 but

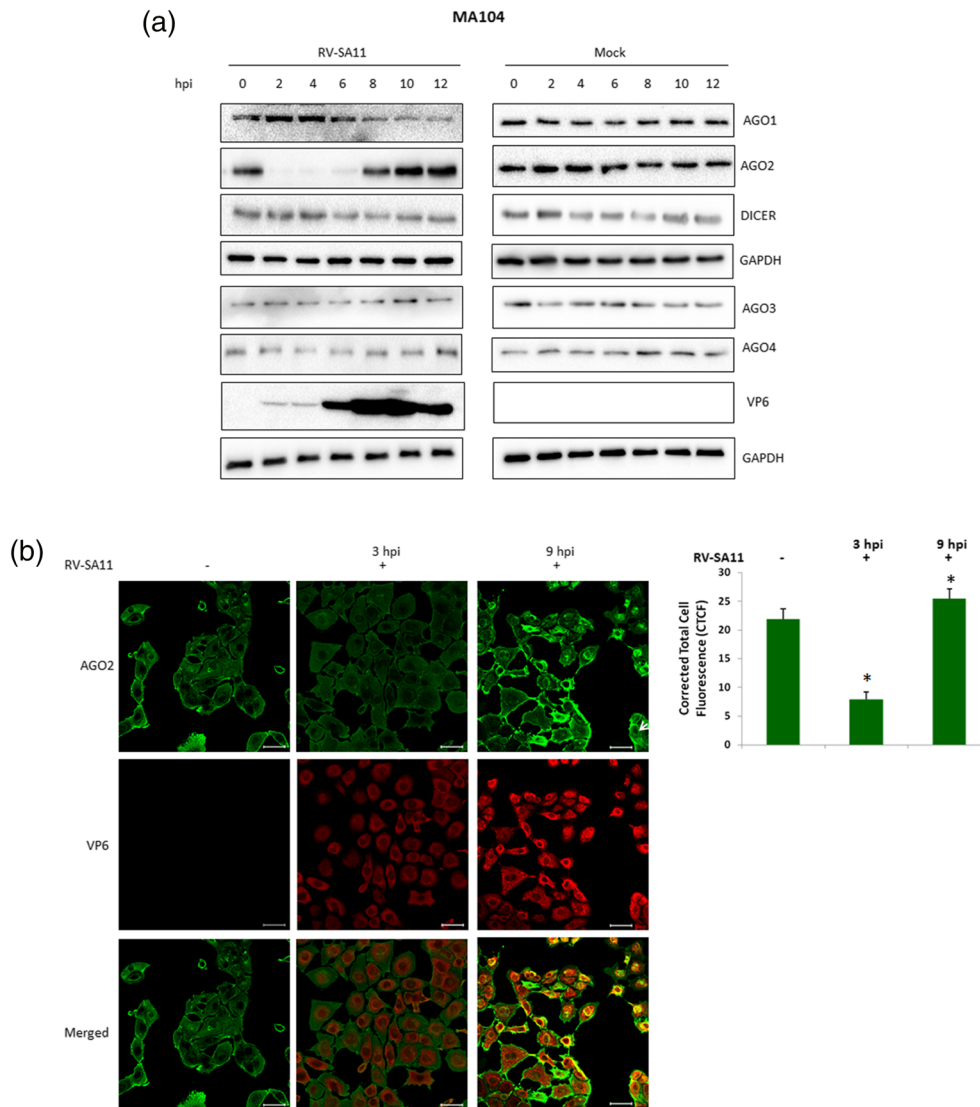


**FIGURE 2** Rotavirus decreases AGO2 protein levels during early hours of infection. (a) MA104 cells were either kept mock infected or infected with RV-SA11 for indicated time points. Whole cellular extracts were prepared and subjected to western blot analysis to check expressions of AGO1, AGO2, AGO3, AGO4, and DICER. (b) MA104 cells, mock-infected, or infected with RV-SA11 were fixed with paraformaldehyde at indicated time points and further stained overnight with anti-AGO2 and anti-VP6 (as a marker of virus infection) antibodies. Secondary staining was done with Dylight 488 labelled anti-rabbit and Rhodamine labelled anti-mouse antibody. Cells were visualised by confocal microscopy (63 $\times$  oil immersion, tiling mode; scale bar 20  $\mu$ M); background normalized AGO2 fluorescence was measured and represented as CTCF (right panel)

not to 1  $\mu$ M of lysosomal inhibitor Bafilomycin A1 (Figure S3D). In addition to the putative E3 ubiquitin ligase activity intrinsic to RV-NSP1, co-opted host E3 ubiquitin ligase complex Cullin has recently been implicated to be interacting with (Ding et al., 2016; Lutz, Pace, & Arnold, 2016) and be involved in mediating proteasomal degradation of host substrates (Davis, Morelli, & Patton, 2017; Ding et al., 2016). Interestingly, inhibition of E3 ubiquitin ligase activity of Cullin by MLN4924 (500 nM) failed to rescue RV-NSP1-mediated reduction in AGO2 levels in MA104 cells (Figure 3d), suggesting AGO2 degradation by RV-NSP1 to be independent of co-opted Cullin machinery. Disappearance of neddylated forms of Cullin1 and Cullin3 confirmed functional inactivation of Cullin E3 ubiquitin ligase in MLN4924-treated cells (Figure 3d). Dispensability of Cullin1 and Cullin3 as the

E3 ubiquitin ligases co-opted by RV-NSP1 for degradation of AGO2 was further validated when AGO2 degradation was not prevented in RV-NSP1-transfected cells cotransfected with dominant negative constructs of Cullin1 and Cullin3 (Figure S3E). To further assess whether proteasomal degradation of AGO2 is preceded by increased ubiquitination, MA104 cells transfected with pCMV-FLAG-Ub were further cotransfected with either pcDNA6B or pcDNSP1; 36-hr posttransfection, equal amount of cell lysates were immunoprecipitated with anti-FLAG antibody, and immunoprecipitates were assessed for the levels of AGO2. Results revealed distinctly increased ubiquitination of AGO2 in the presence of RV-NSP1 (Figure 3e, left panel). Reciprocal coimmunoprecipitation study substantiated ubiquitin enrichment of AGO2 in RV-NSP1-overexpressing cells (Figure 3e,

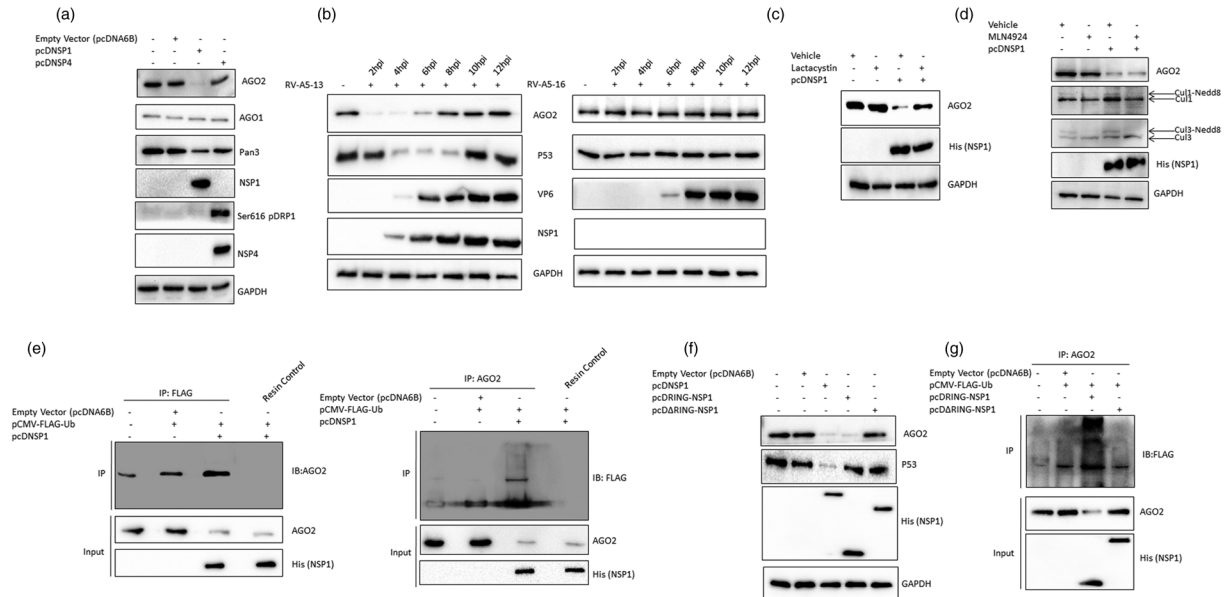


**FIGURE 3** Rotaviral nonstructural protein 1 triggers ubiquitination and proteasomal degradation of AGO2. (a) Whole cellular extracts from pcDNSP1- and pcDNSP4-transfected MA104 cells were subjected to western blot analysis for checking expressions of AGO1, AGO2, Pan3, and Ser616 pDRP1. (b) MA104 cells were mock-infected or infected with RV-A5-13 and RV-A5-16 (2–12 hpi). AGO2 and P53 expression was checked in cellular extracts of infected cells prepared at indicated time points. NSP1 protein expression was analysed in the same lysates to confirm RV-A5-13 and RV-A5-16 infection. (c) MA104 cells were kept untransfected or transfected with pcDNSP1; 6-hr posttransfection, cells were treated with vehicle (DMSO) or 1- $\mu$ M Lactacystin. Cellular lysates prepared after 24 hr of transfection were subjected to SDS-PAGE followed by immunoblotting and expression of AGO2 was checked. His (NSP1) expression was checked as a marker of pcDNSP1 transfection. (d) pcDNSP1-transfected MA104 cells were treated with either vehicle (DMSO) or 500-nM MLN4924 (6 hr after transfection). Whole-cell lysates were prepared (24-hr posttransfection), and immunoblotting was done to check expressions of AGO2, His (NSP1), Cullin1, and Cullin3. Neddylated form of Cullin1 and Cullin3 is indicated by arrows. (e) MA104 cells ectopically expressing pCMV-FLAG-Ub were cotransfected with either empty vector (pcDNA6B) or pcDNSP1. (Left panel) Cellular lysates prepared after 36 hr of transfection were immunoprecipitated with anti-FLAG antibody, and immunoprecipitates were further subjected to immunoblotting with anti-AGO2 antibody. Input lysates were probed with anti-AGO2 and anti-His (NSP1) antibodies. (Right panel) Reciprocal coimmunoprecipitation was done with anti-AGO2 antibody followed by immunoblotting with anti-FLAG antibody. Expressions of AGO2, His (NSP1) were checked in the input lysates. (f) MA104 cells were transfected with either empty vector (pcDNA6B), full-length NSP1 (cloned in pcDNA6B vector), or truncated domains of NSP1 (RING and  $\Delta$ RING domain cloned in pcDNA6B vector). After 36 hr of transfection, cell lysates were subjected to western blot analysis to check levels of AGO2 and P53. Expression of His tag was used as a marker of pcDNSP1, pcDRING-NSP1, and pc $\Delta$ RING-NSP1 transfection. (g) Equal amount of lysates from pCMV-FLAG-Ub overexpressed MA104 cells cotransfected with pcDRING NSP1 or pc $\Delta$ RINGNSP1 were immunoprecipitated with anti-AGO2 antibody. Immunoprecipitates were then probed with anti-FLAG antibody. Simultaneously, His (NSP1) and AGO2 expressions were assessed in the input lysates

right panel). Ubiquitin enrichment of AGO2 was also validated during early hours (at 3 hpi) of RV-SA11 infection by coimmunoprecipitation study (Figure S3F). Notably, ubiquitinated AGO2 levels were found to be low at 9 hpi compared with 3 hpi, justifying their corresponding cellular levels represented in the input lanes (Figure S3F).

Next, we investigated which domain of RV-NSP1 causes degradation of AGO2. MA104 cells were transfected individually with full-length pcDNSP1, pcDRING-NSP1, and pc $\Delta$ RING-NSP1; AGO2 expression was checked 36-hr posttransfection by immunoblot analysis. Results revealed that overexpression of only RING domain of RV-NSP1 was sufficient to cause AGO2 degradation (Figure 3f). Degradation of P53 was simultaneously assessed as a positive control. Consistent to the previous report (Bhowmick et al., 2013), P53 reduction was observed only in the presence of full-length RV-NSP1 but not in the presence of either RING or  $\Delta$ RING domain of NSP1 (Figure 3f). Role of NSP1 RING domain in degrading AGO2 was also validated in HEK293 cell line (Figure S3G). Furthermore, increased ubiquitination

of AGO2 in the presence of only RING domain of NSP1 (Figure 3g) confirmed its role in ubiquitination-mediated proteasomal degradation of AGO2.

## 2.4 | RV nonstructural protein 1 acts as a putative viral suppressor of RNA silencing

The observation that RV-NSP1 can cause proteasomal degradation of AGO2 prompted us to check whether RV-NSP1 can also function as a suppressor of RNA silencing. To evaluate this, Rbx1 protein expression was assessed in MA104 cells transfected with either Rbx1 siRNA alone or pcDNSP1 in addition to Rbx1 siRNA. Immunoblotting revealed inefficient knocking down of Rbx1 expression by siRNA in the presence of RV-NSP1 (Figure 4a). Sensitivity of ectopic GFP (pEGFP-N1) expression to siGFP was also reduced in RV-NSP1-overexpressing cells (Figure S4A), indicating that RV-NSP1 might

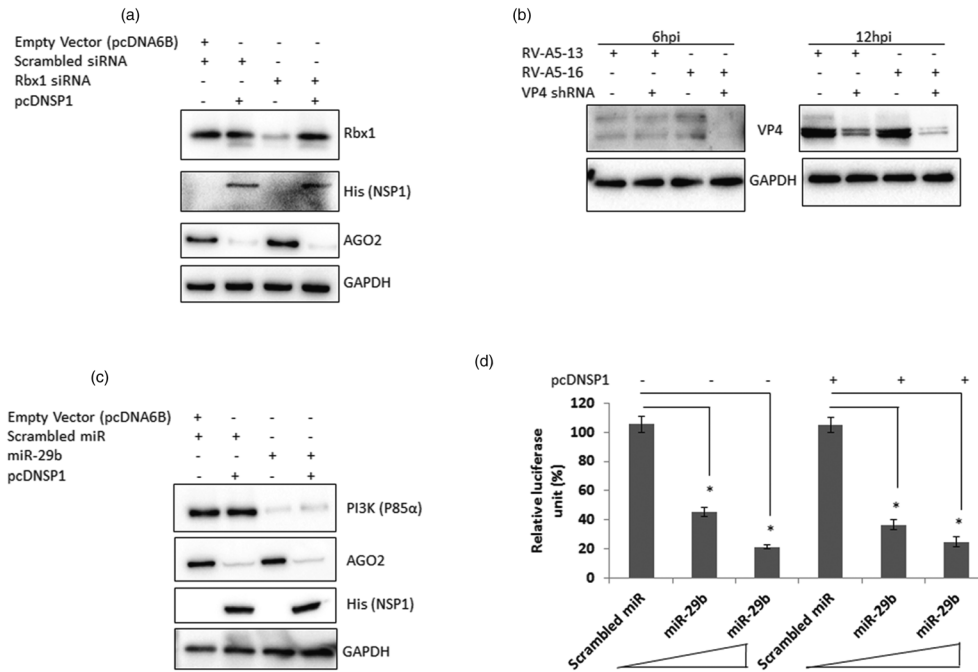


**FIGURE 4** RV-NSP1 acts as a RNA silencing suppressor. (a) MA104 cells were transfected with either Rbx1 siRNA alone or pcDNSP1 in association with Rbx1 siRNA for 36 hr. Subsequently, cellular lysate preparation and western blot analysis were done to check expressions of Rbx1, AGO2, and His (NSP1). (b) Empty vector (PLKO.1-TRC) transfected or VP4-shRNA transfected MA104 cells were infected with RV-A5-13 and RV-A5-16 strains for indicated time points (6 and 12 hpi). Whole-cell lysates were subjected to SDS-PAGE followed by immunoblot analysis to check expression of VP4. (c) MA104 cells were transfected with miR-29b mimic and pcDNSP1 at indicated combinations (marked by + and -). Expressions of P85 $\alpha$ -PI3K and AGO2 were checked in the lysates prepared after 36 hr of transfection. (d) pMIR-REPORT Luciferase construct containing the 3'-UTR of P85 $\alpha$ -PI3K was cotransfected with different doses of miR-29b mimic (20 or 40 nM) in HEK293 cells ectopically coexpressing either empty vector (pcDNA6B) or pcDNSP1. Relative luciferase activity was measured 36-hr posttransfection by normalising Firefly luciferase against corresponding Renilla luciferase control

serve as an RNA-silencing suppressor. Furthermore, silencing of VP4 expression by VP4 shRNA at 6 hpi was observed only in RV-A5-16 (NSP1-mutant)-infected cells but not during RV-A5-13 infection (Figure 4b; Figure S4B). This is consistent to no degradation of AGO2 in A5-16 infected cells compared with sharp degradation of AGO2 in isogenic strain A5-13 during 2-6 hpi (Figure 3b). Functionality of miRNA-mediated RNAi, however, remained unaffected in the presence of RV-NSP1 as observed by the equal competence of miR-29b mimic in attenuating its target (P85 $\alpha$  subunit of PI3K) both in the presence and absence of overexpressed RV-NSP1 (Figure 4c). Furthermore, overexpression of RV-NSP1 in HEK293 cell line cotransfected with escalated concentration of miR-29b mimic could not hinder target (P85 $\alpha$  subunit of PI3K) repression capacity of miR-29b as evident by the luciferase reporter assay data (Figure 4d). Together, the results suggest that RV-NSP1 can be regarded as a putative RV-encoded suppressor of RNAi, which inhibits functionality of siRNA and shRNA but not of miRNA.

## 2.5 | RV nonstructural protein 1 associates with AGO2

We further looked for any possible association between RV-NSP1 and AGO2, which might lead to proteasomal degradation of AGO2 in the

presence of RV-NSP1. pcDNSP1-transfected MA104 cells were lysed 36-hr posttransfection and subsequently immunoprecipitated with anti-His antibody. The presence of AGO2 in the immunoprecipitate indicated an association between AGO2 and RV-NSP1 (Figure 5a). The presence of P53 and absence of AGO1 in the immunoprecipitate served as positive and negative control, respectively, for this interaction assay (Figure 5a). Similar observation was also made in HEK293 cell line (Figure S5A). As both AGO2 (Oceguera et al., 2018) and RV-NSP1 (Hua, Chen, & Patton, 1994) were previously reported to interact with viral RNA, we went on to investigate whether the association between RV-NSP1 and AGO2 required viral RNA intermediates. Interestingly, AGO2-RV-NSP1 association was found to be unperturbed in the presence of both single-stranded RNA-specific RNase I and double-stranded RNA-specific RNase III (Figure 5b), excluding the possibility of viral RNA scaffold to have a mediating role. AGO2 activity has been reported to be regulated by phosphorylation (Bridge et al., 2017; Horman et al., 2013). Phosphorylation of RV-OSU-NSP1 by caesin kinase II has also recently been shown to be a prerequisite for NSP1- $\beta$ TrCP association (Davis et al., 2017). To further explore whether association between RV-NSP1 and AGO2 is influenced by phosphorylation status of either NSP1 or AGO2, coimmunoprecipitation analysis was carried out in the presence of lambda protein phosphatase (lambda PP). NSP1-AGO2 association was not hampered following dephosphorylation of lysates with

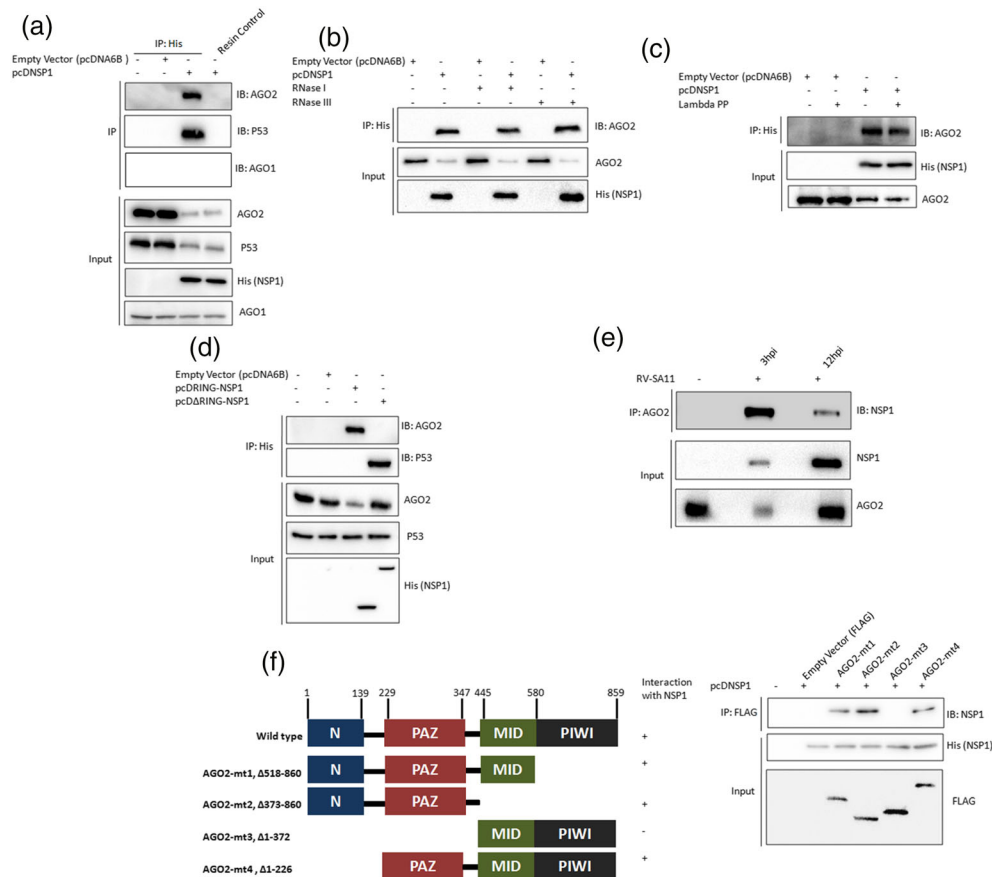


**FIGURE 5** RV-NSP1 associates with the PAZ domain of AGO2. (a) Equal amount of lysates from MA104 cells transfected with either empty vector (pcDNA6B) or pcDNSP1 were subjected to immunoprecipitation with anti-His antibody. Immunoprecipitates were further checked for the presence of AGO2, P53, and AGO1. Probing inputs with anti-AGO2, anti-P53, anti-His, and anti-AGO1 antibodies confirmed protein expressions. (b) Anti-His coupled resin was incubated with cellular extracts from mock-transfected or pcDNSP1-transfected MA104 cells pretreated with RNase I and RNase III. Immunoprecipitates were subsequently subjected to western blot analyses with anti-AGO2 antibody. Input lysates were probed with anti-His and anti-AGO2 antibodies. (c) MA104 cells were transfected with empty vector or pcDNSP1 for 36 hr followed by whole-cell lysate preparation. Cellular lysates were incubated with active lambda PP or heat inactivated lambda PP as described in the Experimental Procedures section followed by immunoprecipitation with anti-His antibody. Expression of AGO2 was analysed in the immunoprecipitates by immunoblot analysis. Expression of AGO2 and His (NSP1) was analysed in the input lysates (d) MA104 cells were transfected with pcDRING-NSP1 or pcDΔRING-NSP1. After 36 hr, cell lysates were immunoprecipitated with anti-His antibody. Immunoprecipitates were then resolved on SDS-PAGE, transferred on to PVDF membrane, and finally probed with anti-AGO2 and anti-P53 antibodies. Expressions of AGO2, P53, and His (NSP1) were checked in the input lysates. (e) MA104 cells were mock infected or infected with RV-SA11 for 3 and 12 hr. Equal amount of lysates were immunoprecipitated with anti-AGO2 antibody followed by immunoblotting with anti-NSP1 antibody. Expressions of AGO2 and NSP1 were checked in the input lysates. (f) (Left panel) Schematic representation of AGO2 mutants showing span of deletion (AGO2-mt1–4). (Right panel) MA104 cells transfected with pcDNSP1 were further cotransfected separately with AGO2 mutants (AGO2-mt1–4). After 36 hr, equal amounts of whole-cell lysates were immunoprecipitated using anti-FLAG antibody. Immunoprecipitates were then subjected to immunoblot analysis with anti-NSP1 antibody. Expressions of His (NSP1) and FLAG (for AGO2 domain mutants) were analysed in the input lysates

lambda PP, suggesting phosphorylation-independent interaction between RV-NSP1 and AGO2 (Figure 5c).

To further find out which domain of RV-NSP1 coimmunoprecipitates with AGO2, MA104 cells transfected individually with pcDRING-NSP1, or pcDΔRING-NSP1 were harvested 36-hr posttransfection and subjected to coimmunoprecipitation experiment. AGO2 was found in the anti-His immunoprecipitate of only pcDRING-NSP1-transfected cells (Figure 5d), suggesting that RING domain of RV-NSP1 associates with AGO2. In agreement with our previous report (Bhowmick et al., 2013), P53 interacted with the

ΔRING domain of NSP1 (Figure 5d) and served as a control for this interaction experiment. Consistently, during early hours of infection (3 hpi), RV-NSP1 was present in the anti-AGO2 immunoprecipitate (Figure 5e), but at later time point (12 hpi), association between AGO2 and RV-NSP1 reduced significantly (Figure 5e). This further confirms correlation between restoration of AGO2 protein levels and RNAi functionality during later hours of RV infection. Indeed, this temporal regulation of AGO2-RV-NSP1 association during infection was found to be insensitive to lambda PP treatment (Figure S5B). Disappearance of the hyperphosphorylated patch of RV-NSP5 in the



input lysates of lambda PP-treated cells confirmed lambda PP enzymatic activity (Figure S5B).

AGO proteins consist of N-terminal (N), PAZ (PIWI/AGO/Zwille), MID (middle), and PIWI (P-element-induced Wimpy Testes) domains (Faehnle & Joshua-Tor, 2010). We therefore went on to characterise the region of AGO2 needed for association with RV-NSP1. Coimmunoprecipitation assay was performed using four FLAG-tagged AGO2 mutants [AGO2-mt1 { $\Delta$ PIWI ( $\Delta$ 518-860aa)}, AGO2-mt2 { $\Delta$ PIWI+ $\Delta$ MID ( $\Delta$ 373-860aa)}, AGO2-mt3 { $\Delta$ N +  $\Delta$ PAZ ( $\Delta$ 1-372aa)}, and AGO2-mt4 { $\Delta$ N ( $\Delta$ 1-226aa)}] (Figure 5f, left panel). Expression of these constructs after transfection was confirmed by immunoblotting with anti-FLAG antibody. Each of the AGO2 mutants was cotransfected with pcDNSP1 in MA104 cells, and cell lysates were further subjected to immunoprecipitation using anti-FLAG antibody. Assessing the presence of RV-NSP1 in each of the anti-FLAG immunoprecipitates showed that deletion of 1-372aa (AGO2-mt3) from N terminus of AGO2 abolishes its ability to coimmunoprecipitate RV-NSP1 (Figure 5f, right panel). Barring AGO2-mt3, the rest of the AGO2 mutants (AGO2-mt1, AGO2-mt2 and AGO2-mt4), which were found to associate with RV-NSP1, contain the PAZ domain

(227-372aa; Figure 5f, right panel). These results suggest that the region of 227-372aa of AGO2 (possibly encompassing the PAZ domain) might be involved in the association with RV-NSP1. To further confirm NSP1-AGO2-PAZ association, MA104 cells ectopically expressing pcDNSP1 were further cotransfected with AGO2 construct containing PAZ domain (FLAG-PAZ, 1-480 aa) or AGO2 construct without the PAZ domain (FLAG-PIWI, 478-860 aa). In agreement with the previous results, NSP1-AGO2 association was found in the presence of FLAG-PAZ but not of FLAG-PIWI, confirming involvement of PAZ domain of AGO2 in association with NSP1 (Figure S5C).

## 2.6 | Overexpression of AGO2 reduces RV progeny yield in vitro

Finally, we assessed the functional significance of AGO2 overexpression during RV infection in vitro. Transfection of hAGO2GFP in increasing concentrations (1, 3, 5, and 7  $\mu$ g) heavily reduced expressions of RV structural (VP1 and VP6) and nonstructural (NSP3)

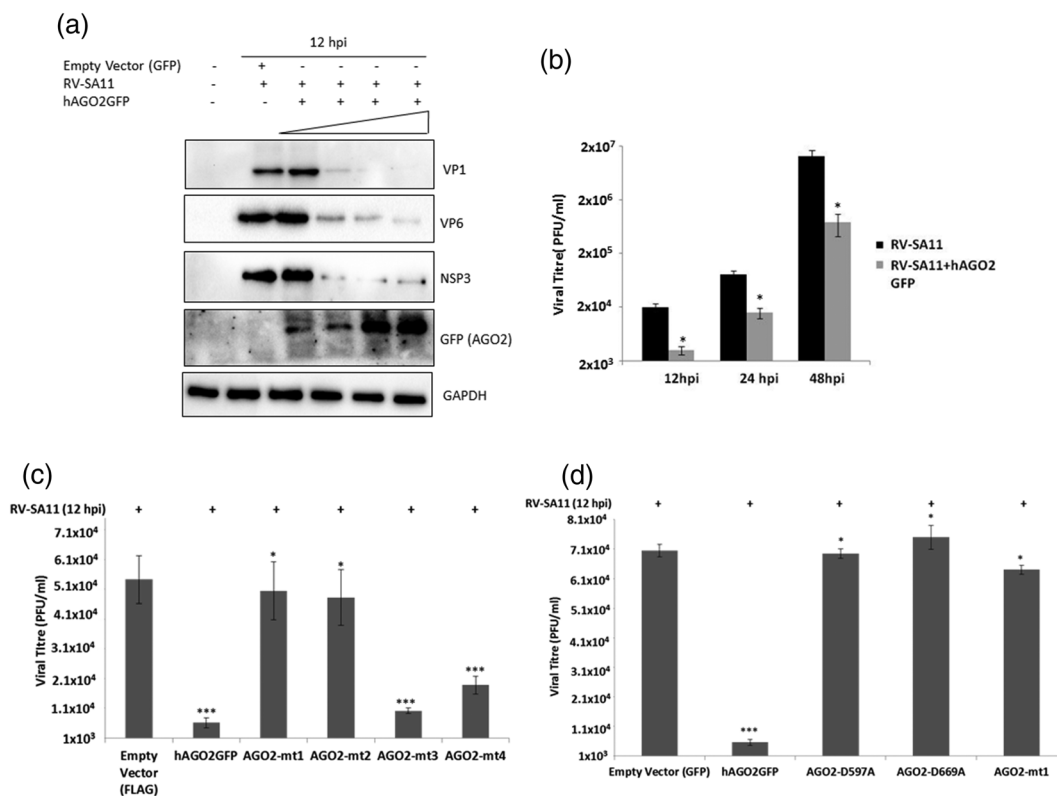


**FIGURE 6** Clonal overexpression of AGO2 reduces viral load in vitro. (a) MA104 cells were transfected with either empty vector (GFP; 5  $\mu$ g) or escalated concentrations of hAGO2GFP vector (1, 3, 5, and 7  $\mu$ g); 36-hr posttransfection, cells were infected (moi 1) with RV-SA11 for 12 hr. Whole-cell lysates were subjected to western blot analyses to check expressions of RV structural (VP1 and VP6) and nonstructural (NSP3) proteins. (b) End point viral titers (12, 24, and 48 hpi) were determined by plaque assay from RV-SA11 (moi 0.5)-infected MA104 cells in the presence and absence of overexpressed hAGO2GFP (5  $\mu$ g) and expressed as virus plaque forming units/ml. (c) MA104 cells were transfected with empty vector (FLAG; 5  $\mu$ g) or AGO2 domain mutants (AGO2-mt1-4) and subsequently infected with RV-SA11 (moi 1; 12 hr). End point viral load was measured by plaque assay and represented as viral plaque forming units/ml. (d) MA104 cells transfected with full-length hAGO2GFP or catalytic-dead AGO2 mutants (designated as AGO2-D597A or AGO2-D669A) were infected with RV-SA11 for 12 hr followed by viral titer measurement. Empty vector (GFP; 5  $\mu$ g) and AGO2-mt1-transfected cells served as negative control and positive control, respectively, for this experiment

proteins in MA104 cells at 12 hpi (Figure 6a) without bystander cytotoxicity (Figure S6A). Concurrently, a dose-dependent reduction in the percentage of RV infectivity was observed at 12 hpi in response to increasing concentration of overexpressed hAGO2GFP (Figure S6B). For further experiments, the concentration of 5  $\mu$ g of hAGO2GFP was chosen, as this concentration showed prominent antiviral effect without stochastic cytotoxicity. Attenuation of RV RNA upon AGO2 overexpression was also significantly prominent at 12 hpi in conventional RT-PCR-based studies (Figure S6C). Moreover, antiviral potency of AGO2 overexpression was found to be evident at as late as 24 and 48 hpi (Figure 6b). Notably, overexpression of AGO1 (GFP Ago1) had no effect on either RV protein expression or RV progeny yield (Figure S6D, E) *in vitro*, further excluding any possibility of GFP-mediated cytotoxicity being the reason of reduced RV infection.

To further identify the domain of AGO2, which has a role in mediating antiviral function, MA104 cells were infected with RV-SA11 in the presence of AGO2 deletion mutants (AGO2-mt1–4); 12-hr postinfection, end point viral titers were measured, and expressions of RV proteins (VP1 and VP6) were analysed. Results showed that all the AGO2 mutants are less potent in exerting antiviral effect compared with the full-length AGO2 (Figure 6c; Figure S6F), suggesting requirement of full-length AGO2 protein for the best antiviral efficacy. Loss of antiviral potency of AGO2, however, is more prominent in the presence of PIWI domain deleted AGO2 mutants (AGO2-mt1 and AGO2-mt2) compared with PIWI domain containing AGO2 mutants (AGO2-mt3 and AGO2-mt4; Figure 6c; Figure S6F). Notably, overexpression of AGO2-mt3 showed slightly yet consistently better anti-rotaviral property than that of AGO2-mt4 (Figure 6c; Figure S6F). Due to lack of PAZ domain, AGO2-mt3 fails to associate with RV-NSP1. Subsequent increased half-life of AGO2-mt3 during infection scenario might be the reason behind better anti-rotaviral property of AGO2-mt3 compared with AGO2-mt4.

AGO2 catalytic activity is reported to be antiviral against a broad range of viral infections (Li et al., 2016). For this purpose, AGO2 site-directed (catalytic-dead) mutants (AGO2-D597A and AGO2-D669A) were transfected in MA104 cells followed by RV-SA11 infection (for 12 hr). End point viral titer measurement showed attenuated RV infection in the presence of slicing-competent wild-type AGO2 to restore in MA104 cells transfected with catalytic-dead AGO2 mutants (Figure 6d). PIWI domain deleted AGO2 mutant (AGO2-mt1) was taken as positive control for this experiment (Figure 6d). Similar results were reflected when expression of RV proteins was checked in the presence of wild type and catalytically impotent AGO2 constructs (Figure S6G). Together, the data suggest that the full-length, slicing-competent AGO2, especially encompassing the PIWI domain, is a critical anti-rotaviral host determinant.

### 3 | DISCUSSION

Physiological relevance of RNAi as an antiviral innate immune measure in plants and nonchordates follows three fundamental lines of arguments: (a) ample viRNAs are produced during natural course of

viral infection in these species, (b) host mutants defective in mounting RNAi-mediated defense response are more susceptible to viral infection, (c) successful viral infection always includes suppression of host RNAi by certain virulence factors called viral-suppressors-of-RNAi (VSRs); VSR-mutant viruses show less virulence in wild-type hosts but acquire important virulence rescue phenotype in RNAi-defective host mutants (Gammon & Mello, 2015; Sledz & Williams, 2005; Younis, Siddique, Kim, & Lim, 2014). In spite of their universality and ubiquitousness, VSRs are highly divergent within and across kingdoms with no sequence homology and have been hypothesised to have evolved independently in different viruses (Burgess, 2013). Viruses-infecting mammalian cells, on the other hand, are only sensitive to synthetic siRNAs that bypass the requirement of Dicer for being processed but produce very little viRNAs during natural course of infection (Cullen & Cherry, 2013). This is possibly due to decreased Dicer-processing activity, which occurs during cellular differentiation perhaps via modification of its internal auto-inhibitory helicase domain. Interestingly, inability to mount RNAi-based innate immunity in response to invading dsRNAs has well been superseded in higher vertebrates by an evolutionary advantageous IFN-based innate immune response. There are, however, contrasting reports on functional coexistence of RNAi and IFN in differentiated somatic cells of mammals. Retention of functional RNAi in IFN-deficient undifferentiated germ cells and embryonic stem cells suggests an attracting hypothesis that RNAi-based antiviral response is subdued in the presence of IFN in higher vertebrates. In favour of this hypothesis is the observation that antiviral RNAi can be experimentally unmasked in mammalian cells upon ablation of the IFN pathway (Maillard et al., 2016). In contrast, there are reports of incompatibility between functional coexistence of RNAi and IFN, as RNAi components are postulated to be proviral and therefore inhibited under certain IFN-rich conditions (Backes et al., 2014).

Cumulative evidences have emerged in support of functional RNAi-dependent antiviral immunity in mammals (Berkhout, 2018; Jeang, 2012; Qiu et al., 2017). According to this view, the very establishment of infection over cellular defence requires production of extremely potent and efficient VSRs. This view is supported by (a) the lack of detectable signature viRNA population in mammalian cells after infection with wild-type viruses and (b) the loss of virulence characteristics of VSR-deficient mutant viruses in mammalian cells owing to the production of abundant viRNAs.

A number of previous reports have enunciated retention of RNAi capability during late hours of RV infection (Arias et al., 2004; Chen et al., 2011; Déctor et al., 2002; Dhillon & DurgaRao, 2018; López et al., 2005; Montero, Rojas, Arias, & López, 2008; Mukherjee et al., 2018; Ocegüera et al., 2018; Patra et al., 2019; Silva-Ayala et al., 2013; Trujillo-Alonso et al., 2011; Yin et al., 2018). Intriguingly, we found infection time point-dependent bimodal regulation of RNAi, where RNAi showed differential sensitivity at early and late hours of RV infection. siRNA-guided RNAi targeting ectopically expressed GFP (Figure 1a,b, Figure S1A, B), and endogenous gene Rbx1 (Figure 1c) and shRNA-mediated RNAi targeting rotaviral vp4 gene (Figure 1d, Figure S1C) were all found to be blocked at early hours of RV-SA11

infection only to regain full functionality at relatively late hours. Evidence of abrogated functionality of synthetic siRNAs suggests that hindered Dicer activity cannot be the exclusive reason for RNAi inhibition during early hours of RV-SA11 infection. In contrast, functionality of miRNA is retained, as miRNA mimics successfully knocked-down target expression both at early and late hours of RV-SA11 infection (Figure 1e,f). This is in agreement with our previous findings, where miRNA mimics preserved their target repression potency in context of RV-SA11 infection (Chanda, Nandi, & Chawla-Sarkar, 2016; Mukhopadhyay et al., 2019). We also did not find global change of miRNA population characteristic of abrogated miRNA biogenesis in our miRNA microarray data (Chanda et al., 2016).

Interestingly, inhibition of siRNA-mediated RNAi 3-hr post RV-SA11 infection coincided with the diminished protein levels of AGO2, but not other AGOs, at that particular time point (2–6 hpi; Figure 2a,b; Figure S2A). AGOs are the catalytic work powers of RISC. Mammals possess four isoforms of AGOs, which share a conserved bilobed structural architecture with four globular domains—the N-terminal lobe consisting of an extreme N-terminal domain followed by a PAZ domain (PIWI-AGO-Zwille), which are separated by a Linker (L1) and a C-terminal lobe with MID (Middle) and PIWI (P body induced wimpy testes) domains. The two lobes are connected by a second Linker (L2) region. The two lobes form a central cleft-like structure with the C-terminal half forming the base of the cleft. In mammalian cells, AGO2 is the only AGO isoform with RNase H-like endonucleolytic activity (slicing) essential for siRNA-mediated target mRNA cleavage (Liu et al., 2004; Rivas et al., 2005; Willkomm, Zander, Grohmann, & Restle, 2016). In the slicing AGO2, the central cleft spanning the PIWI domain harbours the endonucleolytic active site, which cradles the guide and target nucleic acid molecules. AGO proteins are also essential for loading guide RNA onto RISC, where the 5' phosphate terminal of the guide strand is buried in the hydrophilic pocket within the MID domain, and the 3' 2 nucleotide overhang is lodged in the shallow pocket of PAZ domain. The extreme N-terminal domain is involved in unwinding the RNA duplexes. Interestingly, nonslicing AGOs, which are outcompeted by AGO2 when AGO2 is present, may serve redundant functions in AGO2's absence. Therefore, in the absence of AGO2, loading in RISC and miRNA-guided knock-down can be taken over by other nonslicing reserve AGOs to sustain cell viability. In agreement with this is the observation that all AGOs have been shown to bind to miRNAs and siRNAs indiscriminately of sequence, to interact with a common set of helicases and miRNA-binding proteins and to localise to P bodies in mammalian cells (Ruda et al., 2014). Indeed, availability of nonslicing AGOs during early hours of RV infection (Figure 2a, Figure S2A) might be the reason behind retention of miRNA functionality when AGO2 was degraded. It is also noteworthy that inhibition of RNAi correlated with active RV replication as degradation of AGO2 was not observed during infection with UV-inactivated RV (Figure S2B) or in the presence of antiviral agents (such as antiviral siRNAs), which result in overall inhibition of RV replication. Efficient silencing of proviral proteins before the onset of infection abrogates viral infection as a whole thereby jeopardising AGO2 depletion (Bagchi et al., 2012; Chattopadhyay et al., 2017),

which, in turn, may act as a confounding factor for assessing silencing efficiency at postinfective period.

Detailed mechanistic investigations revealed overexpression of RV-NSP1, especially the N-terminal region of RV-NSP1 (Figure 3a,f; Figure S3A, B, G), to trigger protein level reduction of AGO2. RV-NSP1 is a multifunctional protein involved in IFN antagonism, activation of pro-survival PI3K/Akt pathways, denucleating cytoplasmic P bodies, and also harbouring RNA binding as well as cytoskeleton localisation domain (Bagchi et al., 2013; Bhowmick et al., 2015; Ding et al., 2016; Lutz et al., 2016; Morelli, Ogden, & Patton, 2015). IFN antagonistic properties of RV-NSP1 lies in its ability to trigger proteasomal destruction of IRF3, 5, 7, 9,  $\beta$ -TrCP, TRAF2, and RIG-I, whereas P body destabilising property of NSP1 includes degradation of Pan3 by ubiquitin–proteasome system. RV-NSP1 possesses a highly conserved N-terminal RING domain with a zinc-finger motif (C-X2-C-X8-C-X2-C-X3-H-X-C-X2-C-X5-C consensus), which was postulated to have putative E3 ubiquitin ligase activity. In this study, RV-NSP1-mediated AGO2 degradation was prevented in the presence of proteasome inhibitors but not lysosome inhibitor (Figure 3c; Figure S3D). Moreover, ubiquitin enrichment of AGO2 was also observed when full-length or N-terminal region of RV-NSP1 was overexpressed (Figure 3e,g). The role of RV-NSP1 in reducing AGO2 protein levels was further confirmed when AGO2 degradation was observed only during A5–13 infection (a bovine RV strain with wild-type NSP1-containing RING domain [105–246 nucleotides]; cytoskeleton localisation domain [246–531], and IRF3-binding domain [531–981], respectively; Bagchi et al., 2010; Taniguchi et al., 1996) but not in cells infected with A5–16 (NSP1-mutant bovine RV strain, which has a 500-nucleotide deletion from nucleotides 142 to 641 followed by an immediate stop codon at positions 183 to 185, indicating the lack of a functional RING domain and cytoskeleton localisation domain; Taniguchi et al., 1996; Bagchi et al., 2010; Figure 3b). Reciprocal coimmunoprecipitation studies subsequently showed RV-NSP1 to associate with the PAZ domain containing span of AGO2 via its own N-terminal domain independent of any RNA intermediates and residue phosphorylation, justifying degradation of AGO2 in presence of N-terminal domain of RV-NSP1 (Figure 5a–d, F; Figure S5A, C). This is in contrast to the fact that substrate binding specificity of RV-NSP1 generally lies in its highly variable C-terminal half (Lutz et al., 2016; Morelli et al., 2015). The association between AGO2 and RV-NSP1 (Figure 5e, Figure S5B) as well as ubiquitin enrichment of AGO2 (Figure S3F) were also observed at early hour of RV-SA11 infection. Interestingly, at relatively late hours, both association with RV-NSP1 (Figure 5e, Figure S5B) and ubiquitination of AGO2 decreased (Figure S3F), partially explaining restoration of AGO2 protein levels at these late time points of infection.

RV-NSP1 has recently been reported to interact with (Davis et al., 2017; Ding et al., 2016; Lutz et al., 2016) and degrade  $\beta$ -TrCP by co-opting Cullin RING E3 ubiquitin Ligases (CRLs; Ding et al., 2016). Reversal of AGO2 degradation, however, was observed in presence of neither dominant negative forms of Cullin1 and Cullin3 nor pan-Cullin inhibitor MLN4924, suggesting that RV-NSP1-mediated degradation of AGO2 is not dependent on co-opted CRLs

(Figure 3d; Figure S3E). Molecular mechanisms governing time point-dependent bimodal regulation of AGO2-NSP1 association and possible involvement of co-opted host E3 ubiquitin ligase, however, remain to be investigated in future. Moreover, on the basis of our previous observation of p53-NSP1 interaction to get regulated in a similar bimodal fashion (Bhowmick et al., 2013), we also cannot rule out the possibility of mutual inaccessibility of RV-NSP1 or its interaction partner to each other during late phase of infection as a result of differential subcellular localisation. In agreement with Schuster, Tholen, Overheul, van Kuppeveld, and van Rij (2017) and Schuster, Miesen, and van Rij (2019), however, we can make a hypothesis on the physiological relevance of time point-dependent bimodal AGO2 regulation. According to this notion, biphasic AGO2 modulation by RV-NSP1 relies on the prioritisation preference of the latter to get invested either in crippling antiviral RNAi during relatively early phase of infection or antagonising host-triggered antiviral IFN response during the later phase. From the perspective of RV-NSP1 as a putative VSR, degrading AGO2 to disarm si/shRNA-mediated RNAi is advantageous during early hours of infection. But as infection progresses and RV dsRNAs accumulate above a certain threshold, host pattern recognition receptors (RIG1 and MDA5) can start recognising viral replication intermediates as non-self entities and respond by triggering antiviral IFN signalling (Broquet, Hirata, McAllister, & Kagnoff, 2011). To counteract this, RV employs NSP1 to degrade IFN regulatory factors ultimately escaping host immune response. Evidence for viral IFN antagonist to also serve as a VSR is strikingly abundant (Cárdenas et al., 2006; Hartman, Towner, & Nichol, 2004).

VSRs have been reported to interfere at different stages of RNA silencing pathways: viral RNA sensing and dicing, RISC assembly, AGO activity/levels, and also by targeting accessory components of RISC. Most of the VSRs are dsRNA-binding proteins that interact with either Dicer substrates, siRNA duplexes, or both and sequester them away from RNA silencing pathway (Bronkhorst & van Rij, 2014; Schuster et al., 2019). In this respect, it is noteworthy that bacterial dsRNA-binding proteins can also inhibit RNAi pathway non-specifically by virtue of their binding to dsRNAs and thereby withdrawing dsRNAs away from RNAi machinery. There are a few reports of degradation of AGO2 in case of insect and plant viruses (Baumberger, Tsai, Lie, Havecker, & Baulcombe, 2007; Nayak et al., 2018), but no report is available for mammalian viruses. Consistent with the ability of RV-NSP1 to degrade AGO2 proteasomally, RV-NSP1 also showed putative VSR property as its ectopic expression prevented siRNA-mediated RNAi (Figure 4a; Figure S4A). Concurrently, shRNA-mediated RNAi was also found to be functional during early and late hours of A5-16 infection (Figure 4b, Figure S4B). VSR mutant viruses have been shown to be attenuated strains and can only attain high pathogenicity in RNAi-defective host cells. NSP1-mutant RV strain A5-16 has also been reported to have slow growth rate and forms smaller plaques compared with wild-type RV strain A5-13 (Taniguchi et al., 1996; Bagchi et al., 2010). However, the difference in the virulence phenotype between wild-type A5-13 and NSP1 mutant A5-16 may arise, at least partially, from activation of premature apoptosis and failure of IFN antagonism. So, it poses

an experimental challenge to uncouple attenuated pathogenicity stemming from failure to antagonise IFN and premature apoptosis from that due to failure of RNAi inhibition. Indeed, as also observed previously during infection, miRNA mimics retained their functionality in the presence of RV-NSP1 (Figure 4c,d).

Antiviral potency of AGO2 is widely accepted for plant, insect, and mammalian viruses (Alvarado & Scholthof, 2012; Carbonell & Carrington, 2015; Harvey et al., 2011). AGO2 catalytic activity is especially reported to restrict influenza A virus, encephalomyocarditis virus, and vesicular stomatitis virus infection in mammalian cells (Li et al., 2016). In our study too, overexpression of AGO2 but not AGO1 showed potent anti-rotaviral activity (Figure 6a,b; Figure S6 B-E). This is rationally consistent with recent reports of increased RV infectivity in the absence of AGO2 (Dhillon & DurgaRao, 2018; Ocegüera et al., 2018). Moreover, all the functional domains of AGO2 were found to be important for exerting the best antiviral potency, the catalytic PIWI domain being the major determinant (Figure 6c,d; Figure S6F,G) as PIWI domain deleted as well as catalytically dead AGO2 mutants failed to show antiviral effects.

Together, the current findings emphasise how RV hinders RNAi during early hours of infection by prompting degradation of AGO2. Subsequent studies revealed AGO2 to be associating with RV-NSP1 resulting in its ubiquitination and proteasomal destruction independent of co-opted host CRLs. Involvement of RV-NSP1, a classical IFN antagonist, in functioning as a VSR, surprisingly, is not an exception from other mammalian viruses underpinning an interesting and yet-unexplored relationship between the two potential antiviral strategies. It is nonetheless important to mention here that the degree of RV-induced RNAi inhibition, which is attained experimentally by transfecting si/shRNAs way before (36 hr) RV-SA11 infection will vary greatly depending upon the knock-down efficiency of the target achieved prior to infection and also upon the expression kinetics of the target during the period of RNAi inhibition. From the perspective of viral physiology, however, crippling siRNA-mediated RNAi makes sense as signature viRNAs, if indeed produced from the RV genome, would hypothetically be rendered non-functional in the absence of AGO2 during early hours of RV infection and in the absence of abundantly exposed transcriptive/replicative dsRNA substrates beyond that potentially vulnerable early infective phase.

## 4 | EXPERIMENTAL PROCEDURES

### 4.1 | Cell culture and virus infection

The monkey kidney cell line MA104 (ATCC number: CRL-2378™), human embryonic kidney cell line HEK293 (ATCC number: CRL-1573™), and human colorectal adenocarcinoma cell line HT29 (ATCC number: HTB-38™) were grown in Minimal Essential Medium (MEM; 41500034-Gibco, Thermo Fisher Scientific; for MA104) and Dulbecco's Modified Eagle Medium (12800017-Gibco, Thermo Fisher Scientific; for HT29, HEK293) supplemented with 10% (v/v) heat-inactivated Fetal Bovine Serum (10270106-Gibco, Thermo Fisher

Scientific) and 1% (v/v) Antibiotic-Antimycotic (15240062-Thermo Fisher Scientific) within humidified 37°C incubator with 5% CO<sub>2</sub>. Cell culture-adapted RV strains SA11 (simian), A5-13 (bovine), and A5-16 (bovine) were used for this study. Unless otherwise mentioned, cells were infected at a multiplicity of infection (moi) 3 as described previously (Dutta et al., 2011). For all experiments, time of virus addition was taken as 0-hr postinfection (hpi). Mock-infected cells (designated by RV [-]) were treated exactly like infected cells without adsorbing RV and further harvested/fixed along with the last time point of infection (unless otherwise mentioned). For UV inactivation of virus, RV-SA11 was pretreated with 40-µg/ml psoralen AMT for 15 min and then irradiated with long-wave UV light (365 nm) for 2 hr under ice-cold condition (Groene & Shaw, 1992).

## 4.2 | Viral infectivity assay

For calculating viral infectivity, plaque assay was performed as described previously (Dutta et al., 2009). Viral Plaque Forming Units (PFU) were calculated as PFU/ml (of original stock) = 1/dilution factor × number of plaques × 1/(ml of inoculum/plate; Smith, Estes, Graham, & Gerba, 1979). In some experiments, viral infectivity was represented as “percentage of infectivity” of infected test cells compared with infected control cells (infectivity of infected control was considered as 100%).

## 4.3 | Reagents and antibodies

MG-132 (474790-EMD Millipore) and Bafilomycin A1 (19-148-Sigma-Aldrich) were purchased from Merck. Lactacystin (A2583) and MLN4924 (B1036) were purchased from APEX-BIO. RNase I (AM2295-Ambion) and RNase III (AM2290-Ambion) were purchased from Thermo Fisher Scientific. Lambda protein phosphatase (Lambda PP) was purchased from NEB (P0753S). Polyclonal and Monoclonal antibodies used in this study are listed in Table 1. All antibodies were used at manufacturer's recommended dilution. Rabbit polyclonal antibodies against RV-SA11 structural proteins VP1 and VP4 (Komoto et al., 2011) and nonstructural proteins NSP1 (Komoto et al., 2018), NSP3, NSP4, and NSP5 (Komoto et al., 2017) were raised according to standard protocols at the Department of Virology and Parasitology, Fujita Health University School of Medicine, Aichi, Japan.

## 4.4 | Transfection of miRNA mimic and siRNA

Transfection of negative control siRNA (AM4611-Ambion, Thermo Fisher Scientific), Rbx1 siRNA (289686-Thermo Fisher Scientific), and GFP (pEGFP-N1) siRNA (designated as siGFP) (AM4626-Ambion, Thermo Fisher Scientific) was carried out in MA104 and HEK293 cell line using siPORT-NeoFX (Ambion, Thermo Fisher Scientific) according to the manufacturer's instructions. Negative control miRNA mimic (4464058-Thermo Fisher Scientific) and hsa-miR-29b mimic (MC12434-Thermo Fisher Scientific) were transfected in MA104 and HEK293 cell line using Lipofectamine RNAiMAX Reagent (Thermo

**TABLE 1** List of antibodies used in the study

Antibody	Catalog no.	Manufacturer
Argonaute 1	5053	Cell Signaling Technology
Argonaute 2	2897	Cell Signaling Technology
Argonaute 3	5054	Cell Signaling Technology
Argonaute 4	6913	Cell Signaling Technology
Dicer	3363	Cell Signaling Technology
Ub	42895	Cell Signaling Technology
His	12698	Cell Signaling Technology
GFP	1567	Cell Signaling Technology
Caspase 3	9662	Cell Signaling Technology
GSK3β	9315	Cell Signaling Technology
Ser616 pDRP1	44945	Cell Signaling Technology
P53	554165	BD Biosciences
Cul1	sc-135874	Santa Cruz Biotechnology
VP6	sc-101363	Santa Cruz Biotechnology
Pan3	sc-376434	Santa Cruz Biotechnology
GAPDH	sc-25778	Santa Cruz Biotechnology
Cul3	sc-136285	Santa Cruz Biotechnology
Rbx1	sc-393640	Santa Cruz Biotechnology
PI3K (P85α)	sc-1637	Santa Cruz Biotechnology
Anti-VP6	2145	Abcam
Argonaute 2	3409	Abcam
FLAG	F1804	Sigma-Aldrich

Fisher Scientific) according to manufacturer's recommendations. For all transfection experiments, control cells were either kept untransfected and/or transfected with negative control siRNA/miRNA (designated as scrambled siRNA or scrambled miR).

## 4.5 | Plasmids and transfection

pCAG-NSP vectors expressing RV-NSPs of RV-SA11 were gifted by Professor Taniguchi, Department of Virology and Parasitology, Fujita Health University School of Medicine, Aichi, Japan. Full-length NSP1, truncated NSP1 mutants (RING NSP1 [1-82aa] and ΔRING NSP1 [83-482aa]) cloned in pcDNA6B vector and ubiquitin cloned in pCMV-FLAG vector were used as mentioned in the previous study (Bhowmick et al., 2013). dnCul1 (a gift from Wade Harper, Addgene plasmid #15818; Jin, Ang, Shirogane, & Harper, 2005), dnCul3 (a gift from Wade Harper, Addgene plasmid #15820; Jin et al., 2005), GFP-hAGO2 (designated as hAGO2GFP; a gift from Phil Sharp, Addgene plasmid #21981; Leung, Calabrese, & Sharp, 2006), GFP-Ago1 (a gift from Edward Chan, Addgene plasmid #21534; Lian et al., 2009), FDM2 (designated as AGO2-mt1; a gift from Mien-Chie Hung, Addgene plasmid #72209; Shen et al., 2013), FDM1 (designated as AGO2-mt2; a gift from Mien-Chie Hung, Addgene plasmid #72208; Shen et al., 2013), FDM4 (designated as AGO2-mt3; a gift from

Mien-Chie Hung, Addgene plasmid #72211; Shen et al., 2013), FDM3 (designated as AGO2-mt4; a gift from Mien-Chie Hung, Addgene plasmid #72210; Shen et al., 2013) FLAG-PAZ (a gift from Edward Chan, Addgene plasmid # 21529; Lian et al., 2009), and FLAG-PIWI (a gift from Edward Chan, Addgene plasmid # 21543) were obtained from Addgene. Catalytic-dead AGO2 mutants (pcDNA3-AGO2 D597A, pcDNA3-AGO2 D669A) were kind gifts from Greg Hannon (Cancer Research UK, Cambridge Institute). Transfection was carried out in MA104 and HEK293 cell line using Lipofectamine 2000 (Invitrogen) according to the manufacturer's instructions. For all experiments, untransfected and/or empty vector transfected cells were used as controls.

#### 4.6 | RNA isolation, PCR, and quantitative real-time (qRT) PCR

Total cellular RNA was isolated by TRIzol (Invitrogen) according to the manufacturer's instructions. cDNA was prepared from 500 ng of total RNA using Superscript II reverse transcriptase (Invitrogen) and random hexamer by incubating at 42°C for 1 hr. cDNA was amplified by conventional PCR method using specific primers (*vp1*, *vp7*, *vp4*, *nsp3*, *nsp4*, and *nsp1*) as mentioned in the previous study (Banerjee et al., 2018). As a normalising control, *gapdh* was used. PCR amplicons were separated in 0.8–2% agarose gel and visualised using Gel Documentation (Biorad). Real-time PCR reactions were performed in triplicates using SYBR Green (Applied Biosystems) in Step one plus (Applied Biosystems) with primers listed in Table 2. Relative gene expressions were normalised to *gapdh* using the formula  $2^{-\Delta\Delta CT}$  ( $\Delta\Delta CT = \Delta CT_{\text{Sample}} - \Delta CT_{\text{Untreated control}}$ ; CT is the threshold cycle) and represented as “relative expression of RV RNA with respect to mock infected control.”

#### 4.7 | Gel electrophoresis and immunoblot analyses

For western blot analyses, cells were lysed with RIPA buffer. Protein quantitation was done by Bradford assay (Sigma-Aldrich) or Pierce™ BCA Protein AssayKit (Thermo Fisher Scientific). Samples were further boiled in protein sample buffer (final concentration: 50 mM Tris, pH 6.8, 1% SDS, 10% glycerol, 1% β-mercaptoethanol, and 0.01% bromophenol blue) for 20 min before running on SDS-PAGE, transferring onto PVDF membrane and immunoblotting with specific antibodies. Primary antibodies were further identified with HRP conjugated secondary antibody (Pierce) and chemiluminescent substrate

(Millipore). Imaging was done using Image lab software (v5.2.1) in ChemiDoc™MP Imaging System (Biorad). The immunoblots shown are representative of at least three independent experiments. For all experiments, GAPDH was used to confirm equal protein loading and VP6 was used as a marker for RV infection.

#### 4.8 | Luciferase reporter assay

The 3'-UTR luciferase reporter construct of P85α-PI3K was generated by cloning the PCR-amplified human P85α mRNA 3'-UTR (miR-29b target site) into the MluI/HindIII site (3'-UTR PIK3R1-F 5'-AGCTGG AACGCGTATCCCTTCTTTTCTTT-3'; 3'-UTR PIK3R1-R 5'-CAGGCT AAACAAGCTTGACCAAACCTTCT-3') of the pMIR-Report miRNA expression luciferase reporter plasmid (AM5795-Ambion). MA104 and HEK293 cells transfected with luciferase reporter plasmid were further cotransfected with scrambled miR or different doses of mimic miR-29b (20 and 40 nM). Firefly luciferase activity was determined by Dual-Luciferase® Reporter Assay System (E1960-Promega) after normalisation to the expression of control Renilla luciferase.

#### 4.9 | Immunofluorescence

MA104 and HEK293 cells seeded in four-well chamber slides (BD Pharmingen) were treated as mentioned in Figure 1B, S1B, 2B. Cells were then fixed with paraformaldehyde (4% [wt/vol] in phosphate-buffered saline) for 10 min at room temperature and further processed as described previously (Mukherjee et al., 2018). After overnight incubation with primary antibodies (anti-AGO2, anti-NSP5, and anti-VP6) at 4°C, slides were treated with Rhodamine conjugated and DyLight488 conjugated secondary antibodies (Jackson Laboratories, Inc.) for 2 hr in dark at 37°C incubator. Cells were finally stained with Vectashield-DAPI (mounting medium; Vector Laboratories) and examined under Zeiss Axioplan microscope. For CTCF measurement, at least 30 cells from three different fields from three biological replicates were selected, and fluorescence was quantified with ImageJ. For normalisation, background areas with no fluorescence were measured. CTCF was calculated using the formula  $CTCF = \text{Integrated density} - (\text{Area of selected cell} \times \text{mean fluorescence of background readings})$ ; Laget et al., 2017).

#### 4.10 | Coimmunoprecipitation

Lysates from infected/transfected MA104/HEK293 cells were subjected to coimmunoprecipitation using Pierce Co-IP kit (26149) according to the manufacturer's instructions. For Resin controls, cell lysates were incubated with antibody-uncoupled resin and further processed according to the protocol. To immunoprecipitate equal amount of lysates, protein concentration was measured by Bradford assay (Sigma-Aldrich) or Pierce™ BCA Protein AssayKit (Thermo Fisher Scientific). A 5% volume of each lysate was kept as input. To analyse RNA-independent interaction, antibody coupled resins were incubated with equal amount of cell extracts pretreated with RNase III (2 μg/ml)

**TABLE 2** List of primer sequences used for qRT-PCR

Gene Name	Primer name	Sequence
<i>nsp1</i>	<i>nsp1</i> forward	5'GCATGCCAGTTCCTGATGCG3'
	<i>nsp1</i> reverse	5'TGCAAACATGCGGCAATGAGC3'
<i>gapdh</i>	<i>gapdh</i> forward	5'GTCAACGGATTGGTCGTATTG3'
	<i>gapdh</i> reverse	5'TGGAAGATGGTGATGGGATTT3'

or RNase I (1 µg/ml). For analysis of phosphorylation dependent interaction, cellular extracts were incubated with lambda Protein Phosphatase (Lambda PP; 400 U/ml; NEB) in lambda PP buffer, supplemented with 2-mM MnCl<sub>2</sub>. Control reactions contained the same phosphatase that had been inactivated by preheating at 90°C for 15 min (designated as lambda PP[-]). The reactions were incubated for 30 min at 30°C and stopped with addition of 1-mM sodium orthovanadate (Brown & Gordon, 1984). After elution, immunoprecipitates were boiled in SDS-PAGE loading buffer for 20 min followed by gel electrophoresis and immunoblot analyses.

#### 4.11 | Knockdown of VP4 expression by VP4shRNA

Short hairpin sequences targeting VP4 (Forward primer-5'-CCGGAA TGGCGTTAATGACTTCAGTCTCGAGACTGAAGTCATTAACGCCAT TTTTTTG-3'; Reverse Primer-5'-AATTCAAAAAAATGGCGTTAATGA CTTCAGTCTCGAGACTGAAGTCATTAACGCCAT-3') were generated with the siRNA Selection Program hosted by Whitehead Institute for Biomedical Research and inserted into PLKO.1-TRC cloning vector (Addgene plasmid #10878; Moffat et al., 2006). Cells were transfected with VP4 shRNA using Lipofectamine 2000; VP4 knockdown efficiency was assessed by immunoblotting as well as RT-PCR (primer sequence mentioned in Banerjee et al., 2018).

#### 4.12 | Cell viability assay

To determine cytotoxicity of increasing concentrations of hAGO2GFP overexpression in MA104 cells, cell viability assay was conducted. MA104 cells were transfected with increasing concentrations of hAGO2GFP and 36-hr posttransfection MTT assay was done as described in Patra et al. (2019).

#### 4.13 | Statistical analyses

All results are presented as mean ± standard deviation from at least three ( $n \geq 3$ ) independent experiments. Statistical significance of data was analysed by Mann-Whitney test or Student's *t* test using Graphpad Prism 5.0. Statistical significance of data is marked by asterisks ( $p \leq .05$ ;  $**p \leq .01$ ;  $***p \leq .001$ ). *P* value of  $<.05$  was considered to be statistically significant for all experiments.

#### ACKNOWLEDGEMENTS

This study was supported by extramural grant (EMR/2016/001361) from Science and Engineering Research Board; Dept. of Science and Technology (DST-SERB), Government of India and Okayama University Project through Japan Initiative for Global Research Network on Infectious Diseases (J-GRID) of the Agency for Medical Research and Development (AMED). U. M. and U. P. were supported by Senior Research Fellowships from University Grants Commission (UGC) and Indian Council of Medical Research (ICMR) respectively. A. M. was supported by RAMANUJAN research grant SB/S2/RJN-065/2015 from Department of Science and Technology (SERB-DST, India). We

acknowledge Division of Gastrointestinal Sciences at Christian Medical College (CMC), Vellore for providing viral strains and Professor Gregory Hannon (Cancer Research UK, Cambridge Institute) for providing catalytic-dead AGO2 mutants (pcDNA3-AGO2 D597A, pcDNA3-AGO2 D669A). Dr. Asim Biswas is duly acknowledged for his technical assistance in confocal microscopy.

#### CONFLICT OF INTEREST

Authors declare no conflict of interest.

#### ORCID

Mamta Chawla-Sarkar  <https://orcid.org/0000-0002-7141-1785>

#### REFERENCES

- Alvarado, V. Y., & Scholthof, H. B. (2012). AGO2: A new Argonaute compromising plant virus accumulation. *Frontiers in Plant Science*, 2, 112.
- Andersson, M. G., Haasnoot, P. C. J., Xu, N., Berenjian, S., Berkhout, B., & Akusjärvi, G. (2005). Suppression of RNA interference by adenovirus virus-associated RNA. *Journal of Virology*, 79, 9556–9565.
- Arias, C. F., Dector, M. A., Segovia, L., López, T., Camacho, M., Isa, P., ... López, S. (2004). RNA silencing of rotavirus gene expression. *Virus Research*, 102, 43–51.
- Arnold, M. M., Barro, M., & Patton, J. T. (2013). Rotavirus NSP1 mediates degradation of interferon regulatory factors through targeting of the dimerization domain. *Journal of Virology*, 67, 9813–9821.
- Backes, S., Langlois, R. A., Schmid, S., Varble, A., Shim, J. V., Sachs, D., & tenOever, B. R. (2014). The Mammalian response to virus infection is independent of small RNA silencing. *Cell Reports*, 8, 114–125. <https://doi.org/10.1016/j.celrep.2014.05.038>
- Bagchi, P., Bhowmick, R., Nandi, S., Kant Nayak, M., & Chawla-Sarkar, M. (2013). Rotavirus NSP1 inhibits interferon induced non-canonical NFκB activation by interacting with TNF receptor associated factor 2. *Virology*, 444, 41–44. <https://doi.org/10.1016/j.virol.2013.07.003>
- Bagchi, P., Dutta, D., Chattopadhyay, S., Mukherjee, A., Halder, U. C., Sarkar, S., ... Chawla-Sarkar, M. (2010). Rotavirus nonstructural protein 1 suppresses virus-induced cellular apoptosis to facilitate viral growth by activating the cell survival pathways during early stages of infection. *Journal of Virology*, 84(13), 6834–6845. <https://doi.org/10.1128/JVI.00225-10>
- Bagchi, P., Nandi, S., Chattopadhyay, S., Bhowmick, R., Halder, U. C., Nayak, M. K., ... Chawla-Sarkar, M. (2012). Identification of common human host genes involved in pathogenesis of different rotavirus strains: an attempt to recognize probable antiviral targets. *Virus Research*, 169, 144–153. <https://doi.org/10.1016/j.virusres.2012.07.021>
- Banerjee, A., Lo, M., Indwar, P., Deb, A. K., Das, S., Manna, B., ... Chawla-Sarkar, M. (2018). Upsurge and spread of G3 rotaviruses in Eastern India (2014–2016): Full genome analyses reveals heterogeneity within Wa-like genomic constellation. *Infection, Genetics and Evolution*, 63, 158–174. <https://doi.org/10.1016/j.meegid.2018.05.026>
- Barro, M., & Patton, J. T. (2007). Rotavirus NSP1 inhibits expression of type I interferon by antagonizing the function of interferon regulatory factors IRF3, IRF5, and IRF7. *Journal of Virology*, 81(9), 4473–4481. <https://doi.org/10.1128/JVI.02498-06>
- Bartel, D. P. (2009). MicroRNAs: Target recognition and regulatory functions. *Cell*, 136, 215–233. <https://doi.org/10.1016/j.cell.2009.01.002>
- Bartel, D. P. (2018). Metazoan MicroRNAs. *Cell*, 173, 20–51. <https://doi.org/10.1016/j.cell.2018.03.006>

- Baulcombe, D. (2004). RNA silencing in plants. *Nature*, 431, 356–363. <https://doi.org/10.1038/nature02874>
- Baumberger, N., Tsai, C. H., Lie, M., Havecker, E., & Baulcombe, D. C. (2007). The poliovirus silencing suppressor PO targets ARGONAUTE proteins for degradation. *Current Biology*, 17, 1609–1614. <https://doi.org/10.1016/j.cub.2007.08.039>
- Bennasser, Y., & Jeang, K. T. (2006). HIV-1 Tat interaction with Dicer: Requirement for RNA. *Retrovirology*, 3, 95. <https://doi.org/10.1186/1742-4690-3-95>
- Bennasser, Y., Le, S. Y., Benkirane, M., & Jeang, K. T. (2005). Evidence that HIV-1 encodes antiRNA and a suppressor of RNA silencing. *Immunity*, 22, 607–619. <https://doi.org/10.1016/j.immuni.2005.03.010>
- Berkhout, B. (2018). RNAi-mediated antiviral immunity in mammals. *Current Opinion in Virology*, 32, 9–14. <https://doi.org/10.1016/j.coviro.2018.07.008>
- Bhowmick, R., Halder, U. C., Chattopadhyay, S., Nayak, M. K., & Chawla-Sarkar, M. (2013). Rotavirus-encoded nonstructural protein 1 modulates cellular apoptotic machinery by targeting tumor suppressor protein p53. *Journal of Virology*, 87, 6840–6850. <https://doi.org/10.1128/JVI.00734-13>
- Bhowmick, R., Mukherjee, A., Patra, U., & Chawla-Sarkar, M. (2015). Rotavirus disrupts cytoplasmic P bodies during infection. *Virus Research*, 210, 344–354. <https://doi.org/10.1016/j.virusres.2015.09.001>
- Bivalkar-Mehla, S., Vakharia, J., Mehla, R., Abreha, M., Kanwar, J. R., Tikoo, A., & Chauhan, A. (2011). Viral RNA silencing suppressors (RSS): Novel strategy of viruses to ablate the host RNA interference (RNAi) defense system. *Virus Research*, 155(1), 1–9. <https://doi.org/10.1016/j.virusres.2010.10.003>
- Bridge, K. S., Shah, K. M., Li, Y., Foxler, D. E., Wong, S. C., Miller, D. C., ... Ribeiro, P. S. (2017). Argonaute utilization for miRNA silencing is determined by phosphorylation-dependent recruitment of LIM-domain-containing proteins. *Cell Reports*, 20, 173–187. <https://doi.org/10.1016/j.celrep.2017.06.027>
- Bronkhorst, A. W., & van Rij, R. P. (2014). The long and short of antiviral defense: Small RNA-based immunity in insects. *Current Opinion in Virology*, 7, 19–28. <https://doi.org/10.1016/j.coviro.2014.03.010>
- Broquet, A. H., Hirata, Y., McAllister, C. S., & Kagnoff, M. F. (2011). RIG-I/MDA5/MAVS are required to signal a protective IFN response in rotavirus-infected intestinal epithelium. *The Journal of Immunology*, 186, 1618–1626.
- Brown, D. J., & Gordon, J. A. (1984). The stimulation of pp60v-src kinase activity by vanadate in intact cells accompanies a new phosphorylation state of the enzyme. *Journal of Biological Chemistry*, 259, 9580–9586.
- Bucher, E., Hemmes, H., de Haan, P., Goldbach, R., & Prins, M. (2004). The influenza A virus NS1 protein binds small interfering RNAs and suppresses RNA silencing in plants. *Journal of General Virology*, 85, 983–991. <https://doi.org/10.1099/vir.0.19734-0>
- Burgess, D. J. (2013). Small RNAs: Antiviral RNAi in mammals. *Nature Reviews Genetics*, 14(12), 821. <https://doi.org/10.1038/nrg3616>
- Burguán, J., & Havelda, Z. (2011). Viral suppressors of RNA silencing. *Trends in Plant Science*, 16(5), 265–272. <https://doi.org/10.1016/j.tplants.2011.02.010>
- Carbonell, A., & Carrington, J. C. (2015). Antiviral roles of plant ARGONAUTES. *Current Opinion in Plant Biology*, 27, 111–117. <https://doi.org/10.1016/j.pbi.2015.06.013>
- Cárdenas, W. B., Loo, Y. M., Gale, M., Hartman, A. L., Kimberlin, C. R., Martínez-Sobrido, L., ... Basler, C. F. (2006). Ebola virus VP35 protein binds double-stranded RNA and inhibits alpha/beta interferon production induced by RIG-I signaling. *Journal of Virology*, 80, 5168–5178. <https://doi.org/10.1128/JVI.02199-05>
- Chanda, S., Nandi, S., & Chawla-Sarkar, M. (2016). Rotavirus-induced miR-142-5p elicits proviral milieu by targeting non-canonical transforming growth factor beta signalling and apoptosis in cells. *Cellular Microbiology*, 18, 733–747. <https://doi.org/10.1111/cmi.12544>
- Chattopadhyay, S., Mukherjee, A., Patra, U., Bhowmick, R., Basak, T., Sengupta, S., & Chawla-Sarkar, M. (2017). Tyrosine phosphorylation modulates mitochondrial chaperonin Hsp60 and delays rotavirus NSP4-mediated apoptotic signaling in host cells. *Cellular Microbiology*, 19, e12670. <https://doi.org/10.1111/cmi.12670>
- Chen, F., Wang, H., He, H., Song, L., Wu, J., Gao, Y., ... Zhong, J. (2011). Short hairpin RNA-mediated silencing of bovine rotavirus NSP4 gene prevents diarrhoea in suckling mice. *Journal of General Virology*, 92, 945–951. <https://doi.org/10.1099/vir.0.027680-0>
- Cui, L., Wang, H., Ji, Y., Yang, J., Xu, S., Huang, X., ... Chen, Y. (2015). The nucleocapsid protein of coronaviruses acts as a viral suppressor of RNA silencing in mammalian cells. *Journal of Virology*, 89, 9029–9043. <https://doi.org/10.1128/JVI.01331-15>
- Cullen, B. R., & Cherry, S. (2013). Is RNA interference a physiologically relevant innate antiviral immune response in mammals? *Cell Host & Microbe*, 14(4), 374–378. <https://doi.org/10.1016/j.chom.2013.09.011>
- Davis, K. A., Morelli, M., & Patton, J. T. (2017). Rotavirus NSP1 requires casein kinase II-mediated phosphorylation for hijacking of cullin-RING ligases. *MBio*, 8, e01213–e01217.
- Déctor, M. A., Romero, P., López, S., & Arias, C. F. (2002). Rotavirus gene silencing by small interfering RNAs. *EMBO Reports*, 3, 1175–1180. <https://doi.org/10.1093/embo-reports/kvf234>
- Desselberger, U. (2014). Rotaviruses. *Virus Research*, 190, 75–96. <https://doi.org/10.1016/j.virusres.2014.06.016>
- Dhillon, P., & DurgaRao, C. (2018). Rotavirus induces formation of remodeled stress granules and P-bodies and their sequestration in viroplasm to promote progeny virus production. *Journal of Virology*, 92, 24.
- Ding, S., Mooney, N., Li, B., Kelly, M. R., Feng, N., Loktev, A. V., ... Greenberg, H. B. (2016). Comparative proteomics reveals strain-specific  $\beta$ -TrCP degradation via rotavirus NSP1 hijacking a host Cullin-3-Rbx1 complex. *PLoS Pathogens*, 12, e1005929. <https://doi.org/10.1371/journal.ppat.1005929>
- Ding, S. W., Han, Q., Wang, J., & Li, W. X. (2018). Antiviral RNA interference in mammals. *Current Opinion in Immunology*, 54, 109–114. <https://doi.org/10.1016/j.coi.2018.06.010>
- Dutta, D., Bagchi, P., Chatterjee, A., Nayak, M. K., Mukherjee, A., Chattopadhyay, S., ... Chawla-Sarkar, M. (2009). The molecular chaperone heat shock protein-90 positively regulates rotavirus infection. *Virology*, 391(2), 325–333. <https://doi.org/10.1016/j.virol.2009.06.044>
- Dutta, D., Chattopadhyay, S., Bagchi, P., Halder, U. C., Nandi, S., Mukherjee, A., ... Chawla-Sarkar, M. (2011). Active participation of cellular chaperone Hsp90 in regulating the function of rotavirus nonstructural protein 3 (NSP3). *Journal of Biological Chemistry*, 286(22), 20065–20077. <https://doi.org/10.1074/jbc.M111.231878>
- Estes, M. K., & Greenberg, H. B. (2013). Rotaviruses. In D. M. Knipe, P. M. Howley, et al. (Eds.), *Fields virology* (6th ed.) (pp. 1347–1401). Philadelphia PA: Wolters Kluwer Health/Lippincott Williams and Wilkins.
- Faehnle, C. R., & Joshua-Tor, L. (2010). Argonaute MID domain takes centre stage. *EMBO Reports*, 11(8), 564–565. <https://doi.org/10.1038/embor.2010.110>



- Gammon, D. B., & Mello, C. C. (2015). RNA interference-mediated antiviral defense in insects. *Current opinion in insect science*, 8, 111–120. <https://doi.org/10.1016/j.cois.2015.01.006>
- Goubau, D., Deddouché, S., & e Sousa, C. R. (2013). Cytosolic sensing of viruses. *Immunity*, 38(5), 855–869. <https://doi.org/10.1016/j.immuni.2013.05.007>
- Graff, J. W., Ettayebi, K., & Hardy, M. E. (2009). Rotavirus NSP1 inhibits NF $\kappa$ B activation by inducing proteasome-dependent degradation of  $\beta$ -TrCP: A novel mechanism of IFN antagonism. *PLoS Pathogens*, 5, e1000280. <https://doi.org/10.1371/journal.ppat.1000280>
- Graff, J. W., Ewen, J., Ettayebi, K., & Hardy, M. E. (2007). Zinc-binding domain of rotavirus NSP1 is required for proteasome-dependent degradation of IRF3 and autoregulatory NSP1 stability. *Journal of General Virology*, 88, 613–620. <https://doi.org/10.1099/vir.0.82255-0>
- Graff, J. W., Mitzel, D. N., Weisend, C. M., Flenniken, M. L., & Hardy, M. E. (2002). Interferon regulatory factor 3 is a cellular partner of rotavirus NSP1. *Journal of Virology*, 76, 9545–9550. <https://doi.org/10.1128/JVI.76.18.9545-9550.2002>
- Groene, W. S., & Shaw, R. D. (1992). Psoralen preparation of antigenically intact noninfectious rotavirus particles. *Journal of Virological Methods*, 38, 93–102. [https://doi.org/10.1016/0166-0934\(92\)90172-A](https://doi.org/10.1016/0166-0934(92)90172-A)
- Haasnoot, J., De Vries, W., Geutjes, E. J., Prins, M., De Haan, P., & Berkhout, B. (2007). Theebola virus VP35 protein is a suppressor of RNA silencing. *PLoS Pathogens*, 3, 794–803.
- Hannon, G. J. (2002). RNA interference. *Nature*, 418, 244–251. <https://doi.org/10.1038/418244a>
- Hartman, A. L., Towner, J. S., & Nichol, S. T. (2004). A C-terminal basic amino acid motif of Zaire ebolavirus VP35 is essential for type I interferon antagonism and displays high identity with the RNA-binding domain of another interferon antagonist, the NS1 protein of influenza A virus. *Virology*, 328, 177–184. <https://doi.org/10.1016/j.virol.2004.07.006>
- Harvey, J. J. W., Lewsey, M. G., Patel, K., Westwood, J., Heimstädt, S., Carr, J. P., & Baulcombe, D. C. (2011). An antiviral defense role of AGO2 in plants. *PLoS ONE*, 6, e14639. <https://doi.org/10.1371/journal.pone.0014639>
- Horman, S. R., Janas, M. M., Litterst, C., Wang, B., MacRae, I. J., Sever, M. J., ... Qi, H. H. (2013). Akt-mediated phosphorylation of argonaute 2 downregulates cleavage and upregulates translational repression of MicroRNA targets. *Molecular Cell*, 50, 356–367. <https://doi.org/10.1016/j.molcel.2013.03.015>
- Hua, J., Chen, X., & Patton, J. T. (1994). Deletion mapping of the rotavirus metalloprotein NS53 (NSP1): the conserved cysteine-rich region is essential for virus-specific RNA binding. *Journal of Virology*, 68(6), 3990–4000.
- Jeang, K. T. (2012). RNAi in the regulation of mammalian viral infections. *BMC Biology*, 10(1), 58. <https://doi.org/10.1186/1741-7007-10-58>
- Jin, J., Ang, X. L., Shirogane, T., & Harper, J. W. (2005). Identification of Substrates for F-Box Proteins. *Methods in Enzymology*, 399, 287–309. [https://doi.org/10.1016/S0076-6879\(05\)99020-4](https://doi.org/10.1016/S0076-6879(05)99020-4)
- Johnson, K. L., Price, B. D., Eckerle, L. D., & Ball, L. A. (2004). Nodamura virus nonstructural protein B2 can enhance viral RNA accumulation in both mammalian and insect cells. *Journal of Virology*, 78, 6698–6704. <https://doi.org/10.1128/JVI.78.12.6698-6704.2004>
- Komoto, S., Fukuda, S., Ide, T., Ito, N., Sugiyama, M., Yoshikawa, T., ... Taniguchi, K. (2018). Generation of recombinant rotaviruses expressing fluorescent proteins by using an optimized reverse genetics system. *Journal of Virology*, 92, e00588–e00518.
- Komoto, S., Kanai, Y., Fukuda, S., Kugita, M., Kawagishi, T., Ito, N., ... Taniguchi, K. (2017). Reverse genetics system demonstrates that rotavirus nonstructural protein NSP6 is not essential for viral replication in cell culture. *Journal of Virology*, 91, e00695–e00617.
- Komoto, S., Wakuda, M., Ide, T., Niimi, G., Maeno, Y., Higo-Moriguchi, K., & Taniguchi, K. (2011). Modification of the trypsin cleavage site of rotavirus VP4 to a furin-sensitive form does not enhance replication efficiency. *Journal of General Virology*, 92(12), 2914–2921. <https://doi.org/10.1099/vir.0.033886-0>
- Laget, S., Broncy, L., Hormigos, K., Dhingra, D. M., BenMohamed, F., Capiod, T., ... Paterlini-Bréchet, P. (2017). Technical insights into highly sensitive isolation and molecular characterization of fixed and live circulating tumor cells for early detection of tumor invasion. *PLoS ONE*, 12, e0169427. <https://doi.org/10.1371/journal.pone.0169427>
- Leung, A. K., Calabrese, J. M., & Sharp, P. A. (2006). Quantitative analysis of Argonaute protein reveals microRNA-dependent localization to stress granules. *Proceedings of the National Academy of Sciences*, 103, 18125–18130. <https://doi.org/10.1073/pnas.0608845103>
- Li, W. X., Li, H., Lu, R., Li, F., Dus, M., Atkinson, P., ... Palese, P. (2004). Interferon antagonist proteins of influenza and vaccinia viruses are suppressors of RNA silencing. *Proceedings of the National Academy of Sciences*, 101, 1350–1355. <https://doi.org/10.1073/pnas.0308308100>
- Li, Y., Basavappa, M., Lu, J., Dong, S., Cronkite, D. A., Prior, J. T., ... Jeffrey, K. L. (2016). Induction and suppression of antiviral RNA interference by influenza A virus in mammalian cells. *Nature Microbiology*, 2, 16250.
- Li, Y., Lu, J., Han, Y., Fan, X., & Ding, S. W. (2013). RNA interference functions as an antiviral immunity mechanism in mammals. *Science*, 342(6155), 231–234. <https://doi.org/10.1126/science.1241911>
- Lian, S. L., Li, S., Abadal, G. X., Pauley, B. A., Fritzler, M. J., & Chan, E. K. (2009). The C-terminal half of human Ago2 binds to multiple GW-rich regions of GW182 and requires GW182 to mediate silencing. *RNA*, 15, 804–813. <https://doi.org/10.1261/rna.1229409>
- Liu, J., Carmell, M. A., Rivas, F. V., Marsden, C. G., Thomson, J. M., Song, J. J., ... Hannon, G. J. (2004). Argonaute2 is the catalytic engine of mammalian RNAi. *Science*, 305(5689), 1437–1441. <https://doi.org/10.1126/science.1102513>
- López, T., Rojas, M., Ayala-Bretón, C., López, S., & Arias, C. F. (2005). Reduced expression of the rotavirus NSP5 gene has a pleiotropic effect on virus replication. *Journal of General Virology*, 86(6), 1609–1617. <https://doi.org/10.1099/vir.0.80827-0>
- Lu, S., & Cullen, B. R. (2004). Adenovirus VA1 noncoding RNA can inhibit small interfering RNA and MicroRNA biogenesis. *Journal of Virology*, 78, 12868–12876. <https://doi.org/10.1128/JVI.78.23.12868-12876.2004>
- Lutz, L. M., Pace, C. R., & Arnold, M. M. (2016). Rotavirus NSP1 Associates with components of the Cullin RING ligase family of E3 ubiquitin ligases. *Journal of Virology*, 90, 6036–6048. <https://doi.org/10.1128/JVI.00704-16>
- Maillard, P. V., Van Der Veen, A. G., Deddouché-Grass, S., Rogers, N. C., Merits, A., Reis, E., & Sousa, C. (2016). Inactivation of the type I interferon pathway reveals long double-stranded RNA-mediated RNA interference in mammalian cells. *The EMBO Journal*, 35, 2505–2518. <https://doi.org/10.15252/embj.201695086>
- Moffat, J., Grueneberg, D. A., Yang, X., Kim, S. Y., Kloepfer, A. M., Hinkle, G., ... Carpenter, A. E. (2006). A lentiviralRNAi library for human and mouse genes applied to an arrayed viral high-content screen. *Cell*, 124(6), 1283–1298. <https://doi.org/10.1016/j.cell.2006.01.040>
- Montero, H., Rojas, M., Arias, C. F., & López, S. (2008). Rotavirus infection induces the phosphorylation of eIF2 $\alpha$  but prevents the formation of stress granules. *Journal of Virology*, 82(3), 1496–1504. <https://doi.org/10.1128/JVI.01779-07>

- Morelli, M., Ogden, K. M., & Patton, J. T. (2015). Silencing the alarms: Innate immune antagonism by rotavirus NSP1 and VP3. *Virology*, 479, 75–84.
- Mukherjee, A., Patra, U., Bhowmick, R., & Chawla-Sarkar, M. (2018). Rotaviral nonstructural protein 4 triggers dynamin-related protein 1-dependent mitochondrial fragmentation during infection. *Cellular Microbiology*, 20, e12831. <https://doi.org/10.1111/cmi.12831>
- Mukhopadhyay, U., Chanda, S., Patra, U., Mukherjee, A., Rana, S., Mukherjee, A., & Chawla-Sarkar, M. (2019). Synchronized Orchestration of miR-99b and let-7 g Positively Regulates Rotavirus Infection by Modulating Autophagy. *Scientific Reports*, 9(1), 1318. <https://doi.org/10.1038/s41598-018-38473-8>
- Nayak, A., Kim, D. Y., Trnka, M. J., Kerr, C. H., Lidsky, P. V., Stanley, D. J., ... Andino, R. (2018). A Viral Protein Restricts Drosophila RNAi Immunity by Regulating Argonaute Activity and Stability. *Cell Host & Microbe*, 24, 542–557. <https://doi.org/10.1016/j.chom.2018.09.006>
- Oceguera, A., Peralta, A. V., Martínez-Delgado, G., Arias, C. F., & López, S. (2018). Rotavirus RNAs sponge host cell RNA binding proteins and interfere with their subcellular localization. *Virology*, 525, 96–105. <https://doi.org/10.1016/j.virol.2018.09.013>
- Parameswaran, P., Sklan, E., Wilkins, C., Burgon, T., Samuel, M. A., Lu, R., ... Doukas, T. (2010). Six RNA viruses and forty-one hosts: viral small RNAs and modulation of small RNA repertoires in vertebrate and invertebrate systems. *PLoS Pathogens*, 6(2), e1000764. <https://doi.org/10.1371/journal.ppat.1000764>
- Park, S. Y., Lee, J. H., Ha, M., Nam, J. W., & Kim, V. N. (2009). miR-29 miRNAs activate p53 by targeting p85 $\alpha$  and CDC42. *Nature Structural and Molecular Biology*, 16, 23–29. <https://doi.org/10.1038/nsmb.1533>
- Patra, U., Mukhopadhyay, U., Sarkar, R., Mukherjee, A., & Chawla-Sarkar, M. (2019). RA-839, a selective agonist of Nrf2/ARE pathway, exerts potent anti-rotaviral efficacy in vitro. *Antiviral Research*, 161, 53–62. <https://doi.org/10.1016/j.antiviral.2018.11.009>
- Qin, L., Ren, L., Zhou, Z., Lei, X., Chen, L., Xue, Q., ... Hung, T. (2011). Rotavirus nonstructural protein 1 antagonizes innate immune response by interacting with retinoic acid inducible gene I. *Virology Journal*, 8, 526. <https://doi.org/10.1186/1743-422X-8-526>
- Qiu, Y., Xu, Y., Zhang, Y., Zhou, H., Deng, Y. Q., Li, X. F., ... Zhang, F. C. (2017). Human virus-derived small RNAs can confer antiviral immunity in mammals. *Immunity*, 46(6), 992–1004. <https://doi.org/10.1016/j.immuni.2017.05.006>
- Rivas, F. V., Tolia, N. H., Song, J. J., Aragon, J. P., Liu, J., Hannon, G. J., & Joshua-Tor, L. (2005). Purified Argonaute2 and ansRNA form recombinant human RISC. *Nature Structural & Molecular Biology*, 12(4), 340–349. <https://doi.org/10.1038/nsmb918>
- Rojas, M., Arias, C. F., & López, S. (2010). Protein kinase R is responsible for the phosphorylation of eIF2 $\alpha$  in rotavirus infection. *Journal of Virology*, 84, 10547–10466.
- Ruda, V. M., Chandwani, R., Sehgal, A., Bogorad, R. L., Akinc, A., Charisse, K., ... Koteliensky, V. (2014). The roles of individual mammalian argonautes in RNA interference in vivo. *PLoS ONE*, 9(7), e101749. <https://doi.org/10.1371/journal.pone.0101749>
- Samuel, C. E. (2001). Antiviral actions of interferons. *Clinical Microbiology Reviews*, 14(4), 778–809. <https://doi.org/10.1128/CMR.14.4.778-809.2001>
- Schneider, W. M., Chevillotte, M. D., & Rice, C. M. (2014). Interferon-stimulated genes: A complex web of host defenses. *Annual Review of Immunology*, 32, 513–545. <https://doi.org/10.1146/annurev-immunol-032713-120231>
- Schuster, S., Miesen, P., & van Rij, R. P. (2019). Antiviral RNAi in Insects and Mammals: Parallels and Differences. *Viruses*, 11(5), 448. <https://doi.org/10.3390/v11050448>
- Schuster, S., Tholen, L. E., Overheul, G. J., van Kuppeveld, F. J., & van Rij, R. P. (2017). Deletion of cytoplasmic double-stranded RNA sensors does not uncover viral small interfering RNA production in human cells. *MSphere*, 2, e00333–e00317.
- Shen, J., Xia, W., Khotskaya, Y. B., Huo, L., Nakanishi, K., Lim, S. O., ... Hsu, J. L. (2013). EGFR modulates microRNA maturation in response to hypoxia through phosphorylation of AGO2. *Nature*, 497, 383–387. <https://doi.org/10.1038/nature12080>
- Silva-Ayala, D., Lopez, T., Gutierrez, M., Perrimon, N., Lopez, S., & Arias, C. F. (2013). Genome-wide RNAi screen reveals a role for the ESCRT complex in rotavirus cell entry. *Proceedings of the National Academy of Sciences*, 110, 10270–10275. <https://doi.org/10.1073/pnas.1304932110>
- Siomi, H., & Siomi, M. C. (2009). On the road to reading the RNA-interference code. *Nature*, 457, 396–404. <https://doi.org/10.1038/nature07754>
- Siu, R. W., Fragkoudis, R., Simmonds, P., Donald, C. L., Chase-Topping, M. E., Barry, G., ... Fazakerley, J. K. (2011). Antiviral RNA interference responses induced by Semliki Forest virus infection of mosquito cells: Characterization, origin, and frequency-dependent functions of virus-derived small interfering RNAs. *Journal of Virology*, 85, 2907–2917. <https://doi.org/10.1128/JVI.02052-10>
- Sledz, C. A., & Williams, B. R. (2005). RNA interference in biology and disease. *Blood*, 106(3), 787–794. <https://doi.org/10.1182/blood-2004-12-4643>
- Smirnov, Y. A., Kapitulets, S. P., Amitina, N. N., Ginevskaya, V. A., & Kaverin, N. V. (1991). Effect of UV-irradiation on rotavirus. *Actavirologica*, 35(1), 1–6.
- Smith, E. M., Estes, M. K., Graham, D. Y., & Gerba, P. C. (1979). A plaque assay for the simian rotavirus SA11. *Journal of General Virology*, 43, 513–519. <https://doi.org/10.1099/0022-1317-43-3-513>
- Taniguchi, K., Kojima, K., & Urasawa, S. (1996). Nondefective rotavirus mutants with an NSP1 gene which has a deletion of 500 nucleotides, including a cysteine-rich zinc finger motif-encoding region (nucleotides 156 to 248), or which has a nonsense codon at nucleotides 153 to 155. *Journal of Virology*, 70, 4125–4130.
- ten Oever, B. R. (2016). The evolution of antiviral defense systems. *Cell Host & Microbe*, 19(2), 142.
- Trujillo-Alonso, V., Maruri-Avidal, L., Arias, C. F., & Lopez, S. (2011). Rotavirus infection induces the unfolded protein response of the cell and controls it through the nonstructural protein NSP3. *Journal of Virology*, 85, 12594–12604. <https://doi.org/10.1128/JVI.05620-11>
- van Rij, R. P., & Andino, R. (2006). The silent treatment: RNAi as a defense against virus infection in mammals. *Trends in Biotechnology*, 24(4), 186–193.
- Wang, Y., Kato, N., Jazag, A., Dharel, N., Otsuka, M., Taniguchi, H., ... Omata, M. (2006). Hepatitis C virus core protein is a potent inhibitor of RNA silencing-based antiviral response. *Gastroenterology*, 130, 883–892. <https://doi.org/10.1053/j.gastro.2005.12.028>
- Willkomm, S., Zander, A., Grohmann, D., & Restle, T. (2016). Mechanistic insights into archaeal and human Argonaute substrate binding and cleavage properties. *PLoS ONE*, 11(10), e0164695. <https://doi.org/10.1371/journal.pone.0164695>
- Wu, Q., Wang, X., & Ding, S. W. (2010). Viral suppressors of RNA-based viral immunity: Host targets. *Cell Host & Microbe*, 8(1), 12–15. <https://doi.org/10.1016/j.chom.2010.06.009>
- Yin, Y., Dang, W., Zhou, X., Xu, L., Wang, W., Cao, W., ... Peppelenbosch, M. P. (2018). PI3K-Akt-mTOR axis sustains rotavirus infection via the

4E-BP1 mediated autophagy pathway and represents an antiviral target. *Virulence*, 9(1), 83–98. <https://doi.org/10.1080/21505594.2017.1326443>

Younis, A., Siddique, M. I., Kim, C. K., & Lim, K. B. (2014). RNA interference (RNAi) induced gene silencing: a promising approach of hi-tech plant breeding. *International Journal of Biological Sciences*, 10(10), 1150–1158. <https://doi.org/10.7150/ijbs.10452>

Zhu, S., Ding, S., Wang, P., Wei, Z., Pan, W., Palm, N. W., ... Flavell, R. A. (2017). Nlrp9b inflammasome restricts rotavirus infection in intestinal epithelial cells. *Nature*, 546, 667–670. <https://doi.org/10.1038/nature22967>

## SUPPORTING INFORMATION

Additional supporting information may be found online in the Supporting Information section at the end of the article.

**How to cite this article:** Mukhopadhyay U, Chanda S, Patra U, Mukherjee A, Komoto S, Chawla-Sarkar M. Biphasic regulation of RNA interference during rotavirus infection by modulation of Argonaute2. *Cellular Microbiology*. 2019;21:e13101. <https://doi.org/10.1111/cmi.13101>